In vitro investigation of polydopamine-nanoparticles to overcome an intact blood-brain barrier

Vanessa Katharina Augstein

Johannes Gutenberg University, Mainz

Max Planck Institute for Polymer Research, Mainz

Mainz, 2021

Advisors: Prof. Dr. Tanja Weil

Prof. Dr. Walter Stöcker

Supervisor: Dr. Jana Hedrich

Abstract

One of the most challenging hurdles in treating the central nervous system (CNS) is to overcome the blood-brain barrier (BBB). Caused by the BBB, currently therapies for neurological diseases are highly correlated to side effects due to the use of invasive or harmful treatments. In this thesis, the polymers of polydopamine, poly(L-DOPA), and poly(D-DOPA) were analyzed as potential nanoparticles to overcome the BBB within *in vitro* experiments. The first hurdle for the particles is to be uptaken in brain endothelial cells since these cells are building the inner side of the capillary. Therefore, the polymer uptake was analyzed using confocal microscopy for a murine brain endothelial cell line model (bEnd.3). Further, the transport pathway through the endothelial cells and the transportation rates across a confluent monolayer of bEnd.3 cells were investigated. Following the uptake and the neurotoxicity on primary murine neurons was examined. Moreover, the polymers toxicity on the endothelial cells and the neurotoxicity was compared to its monomer.

To summarize this study, the polymers were uptaken into bEnd.3 cells in a concentration-related manner and visible in early endosomes, the cytosol, unknown vesicles, and late endosomes. This is indicating a transcytotic pathway of the polymers in bEnd.3 cells, which is worth to be investigated in more detail. Moreover, the polymers were uptaken into primary murine neurons and astrocytes. The uptake into the neuronal cells was observed at the lowest applied concentration of 50 µg/ml and higher concentrations did not lead to a higher uptake. Therefore, the saturation of the neuronal cells at a concentration of 50 µg/ml is assumed. Additionally, the *in vitro* transport of the polymers from a luminal to an abluminal compartment was quantified. Since the measured transport rates of the polymers were high (around 100 %) and not similar to prior measurements, the experiments has to be repeated. During the transport assay it could be observed by impedance measurements that the polymers do not trigger any cell stress and that the integrity of the barrier (monolayer of bEnd.3) remains intact. Moreover, viability rates of the polymers on neuronal cells in comparison to the monomers revealed less toxicity for poly(L-DOPA), and poly(D-DOPA) compared to the monomers. For endothelial cells polydopamine and poly(D-DOPA) showed less toxicity compared to its monomer. Additionally, a decrease in viability of neuronal cells caused by endotoxins in the polymer samples could be observed, highlighting the need for endotoxin-free polymer batches.

Overall, due to the uptake of the polymer in bEnd.3 cells and neuronal cells, the lower endothelial toxicity of polydopamine and poly(D-DOPA) and neurotoxicity for poly(L-DOPA), and poly(D-DOPA) compared to the monomers, the potential for the polymer remains promising. Therefore, further investigations of the polymers should be done to overcome an intact *in vivo* BBB and to investigate the therapeutic potential of the polymers.

Table of Contents

List of Figures

List of Tables

Abbreviations

araC	cytosine arabinofuranoside
AD	Alzheimers disease
Arach	Arachnoid layer
ATP	Adenosine triphosphate
BBB	Blood-brain barrier
BCECs	Brain capillary endothelial cells
BM	Basement membrane
BV	Blood vessel
CECs	Cerebral endothelial cells
CED	Convection-enhanced diffusion
CNS	Central nervous system
CSF	cerebrospinal fluid
DA	Dopaminergic
DAPI	4',6-diamidino-2-phenylindole
DAYLs	Disability-adjusted life years
DMEM	Dulbeccos modified eagle medium
DMSO	Dimethyl sulfoxide
DOC	Dopa-decarboxylase
bEnd.3	Murine brain endothelial cell lines
Endo	Endothelial cells
EU	Endotoxin units
FD4	FITC-Dextran 4

FUS	Focused ultrasound
GFAP	Glial fibrillary acidic protein
GLUT1	Glucose transporter 1
HBSS	Hanks balanced salt solution
ICV	Intracerebroventricular infusion
JAMs	Junction adhesion molecules
LAL	Limulus Amebocyte Lysate
LAL	Limulus amebocyte lysate
LB	Lewy bodies
LN	Lewy neurites
LPS	Lipopolysaccharide
ml	Mililiter
NPs	Nanoparticles
NVU	Neurovascular unit
Papp	Apparent permeability
PBS	Phosphate-buffered saline
PD	Parkinsons disease
PDA	Polydopamharveyine
PEG	Polyethylene glycol
Pen	Penicillin
Peri	Pericytes
PFA	Paraformaldehyde
PIA	Pial surface

PMN	Polymorphonuclear
PNS	Peripheral nervous system
RT	Room temperature
SAS	Subarachnoid space
SLCs	Solute carriers
Strep	Streptomycin
TEER	Transendothelial electrical resistance
TJ	Tight junctions
WHO	World health organization
ZO-1	zonula occluden

1 Introduction

1.1 Neurological disorders

The World Health Organization (WHO) singed in 2006 a document which presents the Global Burden of Diseases for neurological disorders. It has been shown that "unless immediate action is taken globally, the neurological burden is expected to become an even more serious and unmanageable threat to public health" (WHO 2006). The estimated number of people affected worldwide by neurological diseases is over a billion. Neurological disorders are closely linked to the integrity of the neurovascular unit (NVU) in the brain. The NVU incorporates three main functionalities, the blood-brain barrier (BBB), neuroimmune axis, and regulation of the cerebral blood flow (Neuwelt et al. 2011). They are tightly integrated into brain physiology and a vital role in the pathogenesis of numerous neurological diseases (Neuwelt et al. 2011). It has been published that 6.3 % of total disability-adjusted life years (DAYLs) of the global burden of diseases are neurological disorders (disability-adjusted life years (DALYs) as a measurement of the total number of years lost because of dead or disabilities) (WHO 2006). Together with HIV/ADIS and malignant neoplasm, neurological diseases are having the highest impacts on public health (shown in figure 1). Therefore, scientists are trying to investigate adequate treatments against neurological disorders. An overall goal would be to regulate the endogenous BBB transporters, which can potentially enhance brain drug delivery and prevent pathogenesis and slow the progression of central nervous system diseases. Hence, it is essential to clarify the processes during brain diseases and mainly the NVU dysfunction to develop strategies to deliver therapeutics across the BBB (Neuwelt et al. 2011).

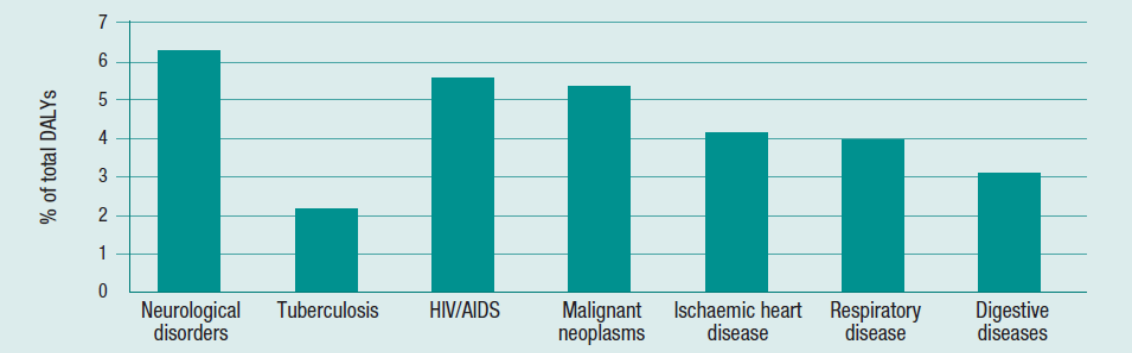

Figure 1: Percentage of total DALYs for selected diseases and neurological disorders
The graph represents the data of total DALYs (total number healthy-life years lost because of death or disabilities) as a measurement of the gap between current health status and an ideal health situation where the entire population lives to an advanced age, free of disease and disability **(**modified from WHO, 2006).

1.2 The human nervous system

The main function of the nervous system is information processing. It consequently receives information about the state of its surrounding, generally about physical or chemical signals. It is separated into the central nervous system (CNS) and the peripheral nervous system (PNS). The CNS includes the brain and the spinal cord. The PNS contains neurons and ganglia cells outside the CNS (Schünke et al. 2015). In this thesis, I will focus on the CNS.

1.3 The central nervous system

The main element of the neuronal system are neurons. Neurons create electrical signals and transport these to other cells. Neurons are built by the soma (perikaryon) and in opposing directions, the shorter dendrite (dendron ancient Greek “tree”), which is often branched, and the more prolonged axon (ancient Greek “axis”). Dendrite and axon are located on the opposite ends of the nerve cell body, which creates a neurons polarization and allows signal transduction. The electrical signal will be transported to the synaptic gap and converted into a chemical signal in the following cell (Schünke et al. 2015).

The second characteristic cell types of the nervous system are glia cells. A particular type of glia cells, called oligodendrocytes, is essential for the signals transportation speed (saltatory excitation). By forming a shell around the axon with myelin layers, the signal can be transported much faster (Schünke et al. 2015). Glia cells also support neurons by controlling the surrounding milieus in the BBB and avoid harmful influences (Schünke et al. 2015). To protect the brains sensitive homeostasis, the brain and the spinal cord lie in a bony shell, the cranial cavity, or the spinal canal. Three membranes, the meninges, envelop the brain tissue and the spinal cord. The brain and spinal cord meninges are embedded in a liquid, the cerebrospinal fluid (Schünke et al. 2015).

The main brain barriers separating blood and CNS are the BBB (NVU of the brain capillaries), the blood-cerebrospinal fluid barrier (epithelia of the choroid plexus), the arachnoid barrier (meninges of the brain), shown in figure 2 (Neuwelt et al. 2011).

1.4 The brain barrier interfaces

The blood-brain barrier can be observed in all organisms with a well-developed CNS and is already present in invertebrates (Abbott 1986).

In the human brain, the barrier is built by endothelial cells, astrocytes, and pericytes, which form the capillaries. The surface of the BBB area is by far the most extensive interface for blood-brain interacting. On an average human, these microvessels surface is between 12 and 18m^2 (Abbott et al. 2010). Therefore, the surface of BBB is highly associated with neurological diseases (e.g. Alzheimers disease (AD), Parkinsons disease (PD), multiple sclerosis, trauma, brain tumors, stroke, and epilepsy (Neuwelt et al. 2011). In addition to the BBB, more interfaces are present, as the blood-cerebrospinal fluid (CSF)-barrier, arachnoid-barrier, and adult ventricular ependyma (shown below in figure 2) (Neuwelt et al. 2011).

During my work, I have investigated nanomaterials, which can overcome an intact BBB. Therefore, I will focus this thesis on the BBB.

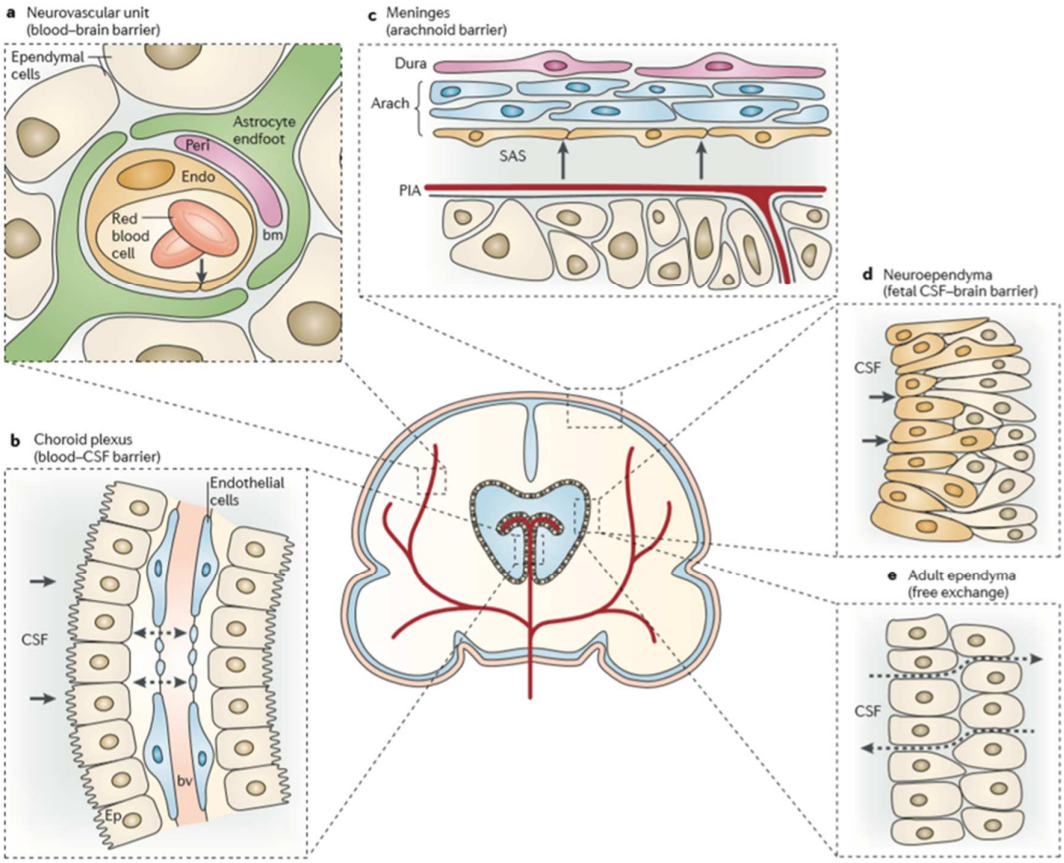

Figure 2: Brain barrier interfaces.
a) Brain endothelial cells (Endo) in the NVU have luminal tight junctions (TJ, shown by the arrow), which form the physical barrier. The endothelial cell and the neighboring pericytes (Peri) are surrounded by the basement membrane (bm). These cells (bm and Peri) are enclosed by the astrocytic end feet, proceeded from nearby astrocytes. b) The endothelial cells of choroid plexus blood vessels are fenestrated and form a non-restrictive barrier (shown by dashed arrows) between the cerebrospinal fluid (CSF) and blood vessel. The arrows on the left are showing the tight apical junctions of the epithelial cells (ep). c) The blood vessels of the Dura in the meninges are fenestrated and provide little barrier function (not shown). The arachnoid layer (Arach) has tight junctions (shown by arrows), and this forms the physical barrier between the CSF-filled subarachnoid space (SAS). Additionally, there are tight junctions in the blood vessels between the arachnoid membrane and the pial surface (PIA) (not shown). d) During early development, the neuroependymal cells are connected by strap junctions (shown by arrows). Those form the physical barrier restricting the passage of larger molecules. e) Compared to the fetal neuroependymal (D), the mature adult ventricular ependyma does not restrict the exchange of molecules (shown by dotted arrows) (Neuwelt et al. 2011).

1.4.1 The blood-brain barrier a challenge for neurological treatments

The blood-brain barrier is built by a monolayer of brain endothelial cells. Additionally, the BBB consists of other cell types as pericytes, smooth muscle cells, end-feed astrocytes, and all are referred to as the neurovascular unit (Neuwelt et al. 2011). The astrocyte end-feet is ensheathing the capillary and connects the neurons (shown in figure 2, a).

The BBB is a highly selective semipermeable barrier that controls the transfer of substances from the bloodstream (peripheral blood) into the brain (CNS). Further, the border is ensuring the transport of essential nutrients and specific biomolecules. It forms a protective and precisely regulated barrier by avoiding blood-borne molecules (possibly toxic), pathogens, and viruses from entering the brain. The main feature of the BBB is tight cell-cell junctions to lower the rate of paracellular diffusion. Additionally, the expression of solute carriers (SLCs) and adenosine triphosphate-binding cassette (ABC) transporters (Keller 2013). Due to the BBBs physicochemical conditions, hydrophilic substances cannot enter the brain (figure 3). Essential hydrophilic substances, as glucose, are transported by a specific insulin-independent transporter (GLUT1) (Schünke et al. 2015). Therefore, small drugs (< 400 Da) are often esterified to make them more lipophilic, to pass barriers like the BBB easier (Schünke et al. 2015).

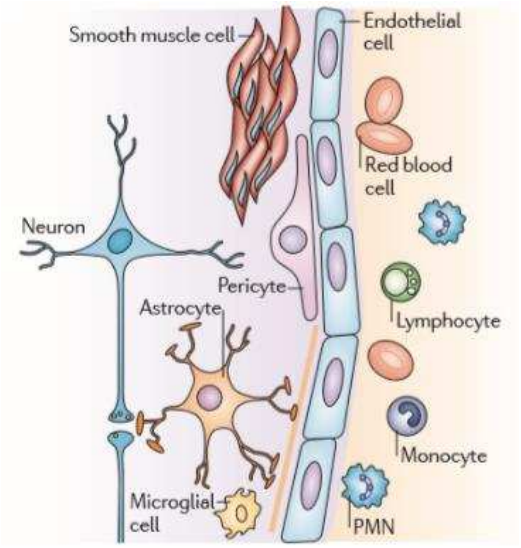

Figure 3: Schematic building of the blood-brain barrier.
The BBB consist of neurons, astrocytes, microglia, pericytes, smooth muscle, and endothelial cells. Tight cell-cell junctions closely connect brain endothelial cells to reduce paracellular diffusion of substances from the bloodstream into the brain. An additional part of this unit is blood cells, particularly polymorphonuclear (PMN) cells, lymphocytes, and monocytes, which interchange with endothelial cells to maintain homeostasis or to respond to inflammation and disease (modified from (Neuwelt et al. 2011)).

1.5 Main compartments of the neurovascular unit

1.5.1 Endothelial cells

The inner side of blood vessels is lined by endothelial cells. During early neural tube development, endothelial cells are entering the brain parenchyma (Keller 2013). Vascularization of the CNS is by angiogenesis by the invasion of endothelial cells from the pre-existing perineural vascular plexus, however this process is not fully understood yet (Kuhnert 2010). While the brain is developing, the neuronal tissue creates the BBB and the brain endothelium characteristics. The endothelium is enveloped from other cell types to ensure the maintenance of the BBB functions. Neurological pathologies are often correlated with dysfunctions of the BBB. This is highlighting the importance of the maintenance of the barrier (Neuwelt et al. 2011).

All endothelial cells are containing cell-cell junctions. The difference between the brains endothelial cells compared to the periphery is the closed ("tighter") junction in the brain. These cell-cell junctions are designed of adherens and tight junctions (TJ) (Keller 2013). Adherens junctions are protein complexes, which connect cells between the actin cytoskeleton and enable mechanical strength (Keller 2013). Tight junctions are designed of a variety of transmembrane proteins, which prevent leakage of transported solutes. The main components are zonula occludens-1 (ZO-1), claudins, occludins, and junction adhesion molecules (JAMs) (Woodfin et al. 2009).

1.5.2 Pericytes

During angiogenesis, the pericytes are entering the brain parenchyma simultaneously with endothelial cells. Pericytes are surrounding the endothelium capillaries, shown in figure 4 (Armulik et al. 2005). The development of pericytes and endothelial cells during angiogenesis is strongly combined. Therefore, dysfunctions or defects in one cell type affect the other cell type (Armulik et al. 2011). By covering 20–30% of the capillary surface, pericytes enhance vessel wall stability to support the brain capillary endothelial cells (BCECs) (Mikitsh and Chacko 2014). Additionally, regulating the expression of endothelial adhesion molecules on the developing vasculature, a regulating immune cell trafficking is potentially given (Daneman et al. 2010). In recent studies, pericytes have been investigated as controllers of endothelial transcytosis in the CNS (Armulik et al. 2010; Daneman et al. 2010; Keller 2013).

1.5.3 Astrocytes

Astrocytes are CNS microglia cells, which are encapsulating the abluminal side of blood vessels with specialized astrocyte end-feeds (covers >98-99 % of the endothelium, shown in figures 2 and 3) (Abbott 2003; Mikitsh and Chacko 2014). In mice, astrocytes differentiate and mature late during development, around birth (Kuhnert 2010). Astrocytes are obligated for several functions as maintaining neuronal homeostasis, free radical scavenging, nutrient uptake/excretion, and ion buffering (Dallas et al. 2006; Mikitsh and Chacko 2014). During development, the astrocytes guideline neurons to their proper place and direct vessels of the BBB. Further, they control the pinocytotic activity and phagocytosis of dead synapses (Keller 2013). Moreover, astrocytes support neuronal activity with oxygen and nutrient supplication (Neuwelt et al. 2011).

1.5.4 Microglia

Before the brain is vascularised, by the invasion of endothelial cells, the microglia cells have been invaded prior (Keller 2013). The reasons why microglia cells are entering the brain parenchyma so early during development is not fully understood. In adults, microglia cells are essential to maintain endothelial integrity by helping damaged vessels and encouraging endothelial repair in homeostasis and pathological conditions (demonstrated in figure 3) (Nimmerjahn 2005; Wynn et al. 2013).

1.6 Transportation across the blood-brain barrier

1.6.1 Passive transport at the blood-brain barrier

Due to the closed tight junctions (TJ), the endothelium is provided with a transport system. This system ensures a specified and controlled transportation of nutrients, ions, and bioactive macromolecules, which is necessary and helps eliminate toxic molecules. Carriers (transmembrane proteins) are mediating the influx of polar molecules into the brain. Therefore, the influx of glucose, amino acids, nucleosides, and neurotransmitters is possible along their concentration gradients (Keller 2013). The energy-independent transportation of molecules from vessel lumen (luminal) to brain parenchyma (abluminal) is possible by paracellular and transcellular diffusion, carrier-mediated transport, and BBB disruption, as displayed in figure 4.

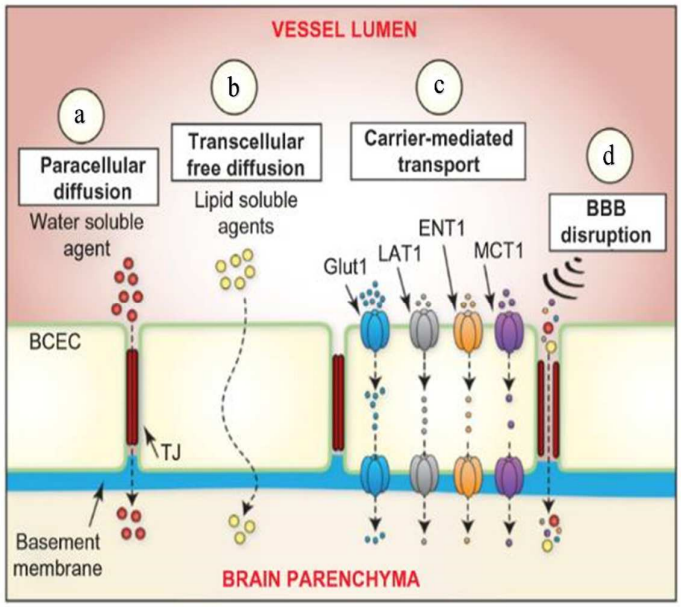

Figure 4: Schematic passive brain uptake mechanisms, across the BBB, from vessel lumen to brain parenchyma.

a) Paracellular diffusion of substances is mainly affected by the size and requires small molecules, to pass through TJs between the brain capillary endothelial cells (BCEC). b) Transcellular free diffusion of small agents. The physiochemical behaviour of the phospholipid membrane of BCECs favours the diffusion of lipid-soluble molecules. Other parameters such as size, lipophilicity, polar surface area, hydrogen bonding potential, and molecular charge affect transcellular free diffusion. c) Carrier-mediated transport along the concentration gradient (energy-independent) of small, specified molecules. d) BBB disruption of the TJs to increase BBB permeability. Afterward, molecules that were unable to diffuse through the phospholipid membrane can easily pass through the disrupted TJs (Mikitsh and Chacko 2014).

1.6.2 Transport at the blood-brain barrier

The brain endothelium expresses a variation of adenosine triphosphate (ATP)-driven efflux pumps (Miller 2010). Efflux pumps transporting molecules against their concentration gradient, which requires ATP (Mikitsh and Chacko 2014). These pumps actively transport substances from the endothelial cells back into the bloodstream or into the brain parenchyma (Dickens et al. 2016). One main BBB efflux transporter and most investigated is p-glycoprotein. This efflux transporter is localized on the luminal side of the brain endothelial cells and is effluxing drugs back into the bloodstream (Dickens et al. 2016). P-glycoprotein has multiple specificities (polyspecific) and regulates the efflux of a wide range of usually prescribed drugs (Keller 2013). A dysfunction of it (e.g. reduced expression) is mainly shown in neurodegenerative diseases (e.g. Alzheimers and Parkinson disease) (Miller 2010).

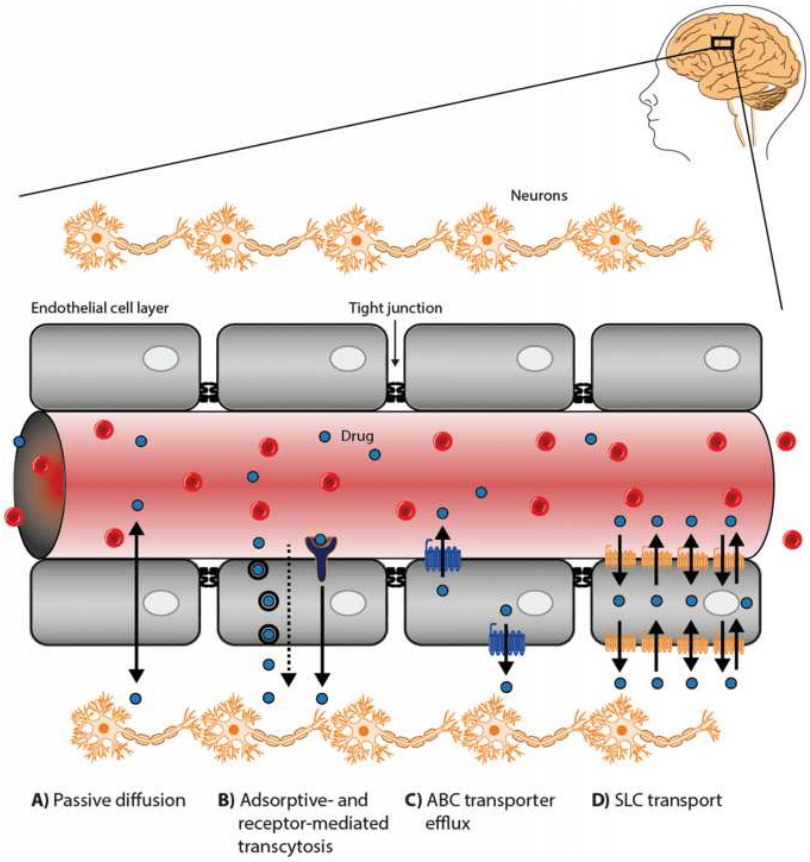

Figure 5: Transport at the blood-brain barrier.
a) Passive diffusion with the concentration gradient through the brain endothelial cells is shown. b) Adsorptive- and receptor-mediated transcytoses is shown. Drug can be transported across by specific receptor-mediated endocytosis and transcytosis pathways. c) ABC transporter efflux. The ABC transporter is actively transporting drugs out of the endothelial cells by utilizing ATP. d) SLC transport. The secondary-active and facilitative transporter can be involved in the carrier-mediated uptake and removal of compounds into and out of the brain (Dickens et al. 2016).

1.7 The current state of research: methods to overcome the blood-brain barrier

At the moment, there a different options for how therapeutics can be transferred into the CNS. One option is to circumvent the barrier after systemic administrations of a drug. Or secondly, by applying it with invasive methods.

1.7.1 Circumvent the barrier

Transcranial brain drug delivery bypasses the BBB by employing three neurosurgical-based delivery methods: intracerebral implantation, intracerebroventricular infusion (ICV), and convection-enhanced diffusion (CED). The main restricting factor for intracerebral and ICV depends on the diffusion of the drug from the application site into the brain parenchyma. At a distance of 0.5mm, the drug concentration is rapidly decreasing by 90% from the depot site. On the other hand, CED consist of liquid convection inside the brain. For an effective penetration, they are maintaining a pressure gradient while the interstitial infusion is necessary. Nevertheless, the brain itself is not developed for a significant intraparenchymal volume flow (Pardridge 2001).

1.7.2 Barrier disruption

The BBB will be disturbed by the opening of tight junctions via osmotic disruption or ultrasound. As a surgical approach, the barrier is physically interrupted by shrinking the brain endothelial cells via osmotic stress. Therefore, hyperosmolar solutions will be applied to leak the blood-brain barrier temporarily. Otherwise, using focused ultrasound (FUS), the maintenance of a selective and local porosity is provided, resulting in an intensification of local delivery inside the brain. Furthermore, the percentage for BBB disrupting can be lowered by combining FUS with intravenously applied lipid-encased perfluorocarbon gas microbubbles. This results in much lower frequencies, which is a less harmful treatment (Bellavance et al. 2008). These techniques include the risk of negative consequences, such as seizures, temporarily altered level of consciousness, and brain herniation. These side effects are intensely harmful to the patients and higher the mortality rate (Kamphorst 2002). Therefore, it is needed to develop a non-invasive, effective, and less harmful treatment for better therapy of neurological disorders and lower the mortality rate.

1.8 The dilemma of Parkinson disease

Parkinson disease (PD) is a movement disorder where the dopaminergic (DA) neurons of the midbrain undergo degeneration (Spillantini 1997; Trépanier et al. 2000; Bridi and Hirth 2018). It is one of the most common neurodegenerative diseases (Kalia et al. 2015). The risk of developing PD is increasing by age. Hence it is declared as an adult-onset and progressive disorder. Mostly, the trigger of the disease is unknown. A genetic cause could be possible in some cases, for example, mutations in the PINK1, parking, and α-synuclein genes (Balestrino and Schapira 2020).

Regardless of the diseases causes, it is driven by the loss of dopamine-producing neurons in the substantia nigra (SN). There are two parts of SN on each hemisphere of the midbrain, a component of the basal ganglia. These two parts of the SN are characterized as the darker pars compacta (SNpc) and the more reddish pars reticulata (SNpr) (Schünke et al. 2015). The basal ganglia have various functions. It unites brain regions (subcortical nuclei) and is mainly associated with the control of movements, and therefore the connection to the motor system (motor cortex) (Balestrino and Schapira 2020).

Therefore, the pathological hallmarks are intracellular inclusions, rich in proteins, named Lewy bodies (LB) and Lewy neurites (LN). LB and LN "are mostly formed of misfolded and aggregated forms of the presynaptic protein α-synuclein (α-syn)" (Spillantini 1997; Trépanier et al. 2000; Bridi and Hirth 2018). After staining the eosinophilic Lewy bodies (LB), round inclusions underneath the microscope are visible. These inclusions consist of the protein α-synuclein, which is only seen in the damaged SN neurons before they degenerate. Currently, the function of α-synuclein is undiscovered, along with the presence of LB (Balestrino and Schapira 2020).

In healthy patients, the SNpc contains dopaminergic neurons and forms the nigrostriatal pathway. Therefore, the SNpc supplies the striatum with information and dopamine (also called the dopamine pathway), which excites the cerebral cortex and triggers movement (Bridi and Hirth 2018; Balestrino and Schapira 2020). Typically for PD patients is caused by the SNpc neurons degeneration, a hypokinetic or low movement state. It has been investigated that regardless of the regression (linear or exponential, between neuronal loss compared to the duration of disease), the appearance of motor signs is by 29% neuronal loss and the loss of 31% dopaminergic fibers (Hilker et al. 2005; Greffard et al. 2006). According to this data, it has been assumed that around 30% of total SN neurons are lost, in comparison to age-matched controls, before the first motor symptoms are appearing (Greffard et al. 2006).

Further, the SN is not only initiating movements, it calibrates and fine-tunes the way how they happen. At first, the tremor, an involuntary shakiness (mostly in the hands), is noticeable. This is called a “resting tremor”, which is present at rest and disappears with intentional movement (Bridi and Hirth 2018; Balestrino and Schapira 2020). Additionally, bradykinesia a slow movement, hypokinesia, a lessened movement, or akinesia, the absence of movement is seen in PD (Bridi and Hirth 2018; Balestrino and Schapira 2020). All three result in difficulty initiating movements. A late feature is postural instability which causes balance problems (Balestrino and Schapira 2020).

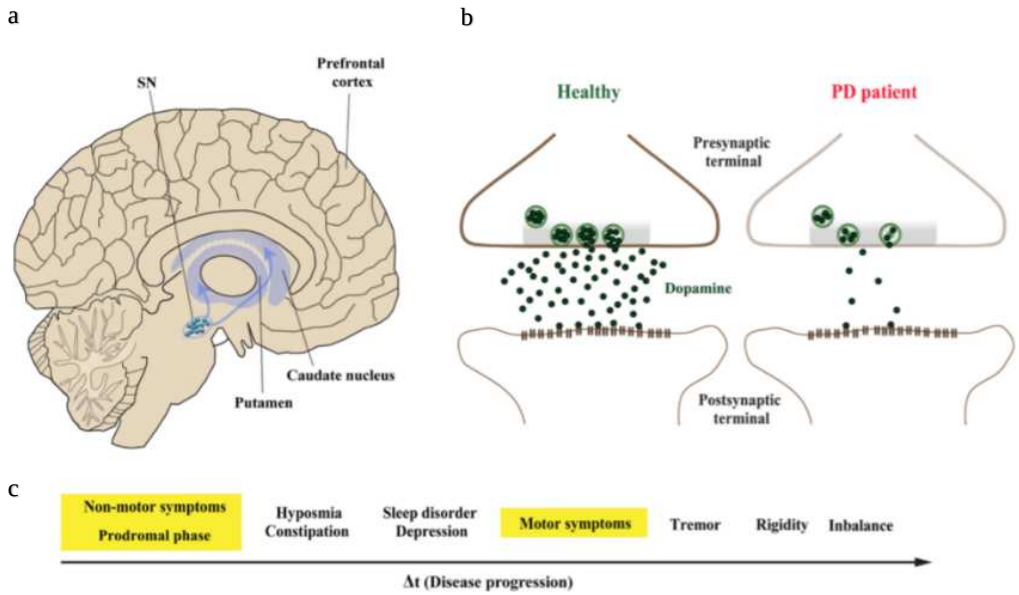

Figure 6: Hallmarks of Parkinson disease
a) Parkinson disease (PD) is characterized by the degeneration of dopaminergic (DA) neurons in the substantia nigra (SN). A dysfunction in PD patients leads to the loss of dopaminergic neurons and following the nigrostriatal pathways decay, which innervates the caudate nucleus and the putamen, which form together with the striatum. Therefore, messages to the striatum cannot be sent via neurons rich in dopamine, which would stimulate the cerebral cortex and initiate movement. b) On the left, the healthy control is shown, compared to a PD patient on the right. As a result of the undergo from the nigrostriatal pathway, the neurotransmitter dopamine on synaptic terminals of striatal neurons is drastically decreasing. c) Motor symptoms are appearing by approximately 30–60% of striatal DA neurons are already dead. For PD patients, it is possible to experience non-motors symptoms 20 years before the onset of motor abnormalities in the so-called prodromal phase, these include olfactory dysfunction, sleep disturbances, and depression (Bridi and Hirth 2018).

1.9 Ultrasmall polydopamine-polyethylene glycol nanoparticles for cellular delivery

The advantages of polymeric nanoparticles have already been revealed. Because of their large quantity of chemical adjustment, besides controlling their relative sizes, they have gained interest in applications in the biomedical field (Harvey et al. 2018). S. Harvey and colleagues published 2018 the synthesis of polydopamharveyine (PDA) polyethylene glycol (PEG) crosslinked copolymer (PDA-PEG) nanoparticles. The amine-terminated PEG3000 [PEG3000(NH2)2] reacted with polydopamine intermediates and crosslinked PDA-PEG nanoparticles with sizes of less than 50nm (Harvey et al. 2018). PEG reduces sedimentation and contributes to improved nanoparticle stability in an aqueous solution, whereas PDA serves as a crosslinker, offering the required functionalities for crosslinking and post functionalization (Harvey et al. 2018). Therefore, the NP was stable in buffer solution without sedimentation, and chemical functionalization was possible, demonstrated by the attachment of fluorescent dyes (Harvey et al. 2018). By cell imaging, a high cellular uptake via energy-dependent endocytosis processes and low cellular toxicity were observed, revealing promising features for cellular imaging and drug delivery applications (Harvey et al. 2018).

1.10 Nanoparticles to improve treatment in Parkinson disease

As explained prior, levodopa (L-DOPA) is the standard treatment to treat PD. The method is causing several side effects, for example, involuntary shakiness called dyskinesia. Therefore, more adequate and less harmful treatments are currently investigated.

The group of Nagasaki published in 2020 the uptake of poly(L-DOPA) particles of primary neurons in a mouse model, with the aim to liberate L-DOPA gradually. They could improve the treatment in a PD model and suppressed the side effects of dyskinesia caused by L-DOPA administration (Vong et al. 2020).

Although, the group could not show and demonstrate the mechanisms of drug delivery to the brain or release and metabolism of poly(L-DOPA). Given the low rate of L-DOPA uptake during the standard PD treatment and the not well understood uptake, drug release, and metabolism of the poly(L-DOPA) nanoparticles, it is essential to investigate uptake mechanisms, drug release, and metabolism of polydopamine and poly(L-DOPA) particles in more details. And to develop the next generation polydopamine or poly(L-DOPA) nanoparticles for effective treatment of Parkinsons disease.

The group of Ciofani showed a lipid-coated polydopamine nanoparticle (L-PDNP) as an antioxidant and neuroprotective agent, which can stimulate neuronal activity (Battaglini et al.

2020). In neurological disorders, oxidative stress is a common issue and leading to neuronal loss and cellular death. L-PDNPs demonstrated the potential to combat the accumulation of reactive oxygen species (ROS) and hinder mitochondrial ROS-induced dysfunction and stimulated neurite growth (Battaglini et al. 2020). Also, the photothermal conversion capacity of L-PDNPs was used to raise the intracellular temperature of neuron-like cells by laser stimulation in the near-infrared (NIR). It has been shown that the temperature rise caused by the NIR stimulation of L-PDNPs can generate a Ca^{2+} influx into human neuroblastoma cells (SH-SY5Y) (Battaglini et al. 2020).

The Choudhury group was also able to minimize oxidative stress and agglomeration of α-synuclein (α-syn) using a biocompatible polydopamine nanocarrier for metformin delivery (Met-encapsulated PDANPs), which can cross the blood-brain barrier in experiments *in vitro*, 3D, and *in vivo* PD models (Sardoiwala et al. 2020). The group could downregulate phospho-serine 129 (pSer129) α-Syn, leading to decreased oxidative stress, prevention of apoptosis, and anti-inflammatory activities (Sardoiwala et al. 2020). The neuroprotective mechanism demonstrated a novel interaction between ubiquitination, mediated by the epigenetic regulator EZH2, and the proteasomal degradation of aggregated pSer129-α-Syn (Sardoiwala et al. 2020). The group showed the neuroprotective function of Met-loaded PDANPs by reversing neurochemical deficits by confirming an epigenetically mediated nanotherapeutic approach to PD prevention (Sardoiwala et al. 2020).

1.11 Aim of study

The blood-brain barrier is the biggest hurdle to overcome in order to treat neurological disorders. It is currently challenging to adequately treat patients with neurological disease, even if known, the high social impacts due to morbidity and mortality. Therefore, nanoparticles (NPs) for non-invasive neurological treatments are currently investigated. Promising nanoparticles for neurological treatments must be able to cross an intact blood-brain barrier (BBB), should reach the target cells, and should show low toxicity.

This work aimed to analyze the polydopamine, poly(L-DOPA), and poly(D-DOPA) polymers potential for neurological treatments. The following scientific questions were addressed:

(1) Are polydopamine, poly(D-DOPA), and poly(L-DOPA) uptaken into endothelial and neuronal cells and transported *in vitro* from luminal (blood side) to abluminal (brain side)?

(2) How are the polymers transported?

(3) Does the polymers influence the integrity of the BBB and the viability of the neurovascular unit (NVU) cells also in comparison to the respective monomers?

These questions have to be investigated in order to evaluate the potential of the herein investigated polymers to develop strategies for neuronal disease treatment, like for example Parkinsons disease.

2 Material and Methods

2.1 Currently used method to treat Parkinson disease

The standard gold treatment for PD is levodopa (L-DOPA) administration to the patient. L-DOPA can cross the BBB and inside the brain parenchyma, converted to dopamine catalyzed by dopa-decarboxylase (DOC) (B. Sampaio-Maia et al.; Cheng et al. 2010; Meiser 2013). Therefore, the lack of dying dopaminergic (DA) neurons in the midbrain is compensated by replacing dopamine. But only 1% of the administered L-DOPA reaches the intact brain (Vong et al. 2020). This leads to the administrations of a high dose of L-DOPA. Controversy, it is known the toxic effects of L-DOPA on neurons. Therefore, several side effects in long-term and high-level administration of L-DOPA are shown. The treatments negative impacts are dyskinesia, stomatitis, sleep disturbance, anxiety, and depression (Vong et al. 2020).

Comparing PD therapy with L-DOPA to patients without the treatment, decreasing the symptoms, and increasing the patients lifespan could be observed. Therefore, the cure is slightly beneficial, although the side effects are still challenging (Vong et al. 2020).

2.2 Blood-brain barrier in vitro models for evaluation of the crossing capability of nanomaterials

Whilhelm and Krizbai described in their review article that the best way to study the BBB is *in vivo*. Besides, *in vivo* experiments are becoming more expensive and less suitable for medium or high throughput screening, the development of advanced BBB *in vitro* models provided a simple and efficient way to study BBB functions and drug discovery (Wilhelm and Krizbai 2014). Mostly, *in vitro* models fulfill the criteria required by the pharmaceutical industry. A difficult challenge is to find a compromise between simplifying models and their cost, capacity, time, and predictive value (Wilhelm and Krizbai 2014). Parameters for a good BBB model are mostly reproducibility, low paracellular permeability, and functional transporters expression. Therefore, transendothelial electrical resistance (TEER) measurement and apparent permeability (Papp) of marker molecules represent the two most important criteria. To improve the *in vitro* modeling, many models with different cell types have been investigated. The simplest ones are monocultures of cerebral endothelial cells on microporous membranes. The membrane pores allow the exchange of solutions between the compartments, but the major disadvantage is the absence of stimulating factors derived from other NVU cellular components (Wilhelm and Krizbai 2014).

Therefore, co-culture models have been developed to mimic the *in vivo* anatomy of the NUV inducing and maintaining barrier properties.

There is a variety of endothelial cells available, which could be used for BBB *in vitro* models. The first choice for drug permeability studies in primary cultures, with cells dissection from an animal. In this case, primary brain endothelial cells seem to be the best concerning the barriers tightness. Because of the complications of the isolation of primary cells and the costs and the quality of different batches, the use of reliable brain endothelial cell lines is accepted (Wilhelm and Krizbai 2014). One major problem of the cell lines is the low barrier property. A standard cell type with good properties such as low permeability and a high TJ expression are bEnd.3 cells.

Overall, every model has its advantages and disadvantages, and a suitable and appropriate model has to be selected based on the specific study (Wilhelm and Krizbai 2014; Moscariello 2018).

2.3 Protocol for blood-brain barrier b.End. 3 Cell Line

2.3.1 Overview

The bEnd.3 endothelial cell line has been widely used for blood vascular research. This cell line is generated from mouse endothelial brain cells, forming the lumen of the brains vessels. The bEnd.3 murine cell line (American Type Culture Collection, Manassas, VA, USA) was cultured as recommended by the manufacturer (Montesano et al. 1990). Cells were cultivated at a humidified atmosphere with 37 °C, and 5 % CO2 in dulbeccos modified eagle medium (DMEM, GlutaMAX, gibco by life technology, Darmstadt, Germany) supplemented with 15 % fetal calf serum (Biochrom, S0115) and 1 % penicillin/ streptomycin (Pen/Strep) (Invitrogen GmbH, Karlsruhe, Germany).

2.3.2 Subculturing of the bEnd.3 cells

At first, the bEnd.3-medium and trypsin-EDTA were pre-warmed (37°C). The bEnd.3 cell line does not need a coating tissue on the culture flask. Every culture flask (T75) was labeled with the date, name, cell line, and cell passage. The new T75 flask was prepped with fresh 20 ml DMEM and stored in the incubator. The culture flask with the cells was washed twice with each 10 ml PBS buffer. After washing, 5 ml (pre-warmed, 37°C) trypsin-EDTA was added and incubated for 3-5 minutes at 37 °C. Circumspectly the cells were checked underneath the microscope during the incubation time. Trypsin-EDTA detaches and separates the adherent

growing cells from the bottom of the culture flask. When the cells are detached and floating in the suspension, the reaction was stopped by adding twice as much of the volume of the medium (10 ml) as trypsin-EDTA. Afterward, the total volume of 15 ml suspension (trypsin-EDTA (5ml) and bEnd.3-medium (10 ml) plus cells) was transferred into a sterile 50 ml falcon tube. The falcon was centrifuged at 200 x g, 21 °C for 5 minutes. The supernatant was discarded as much as possible, without any loss of the cells. Following the pellet was resuspended in 3 ml pre-warmed bEnd.3-medium in a splitting rate of 1:20.

2.3.3 Cryopreservation of bEnd.3 cells

For cryopreservation of bEnd.3 cells, the procedure was followed to the prior describe subculturing of the cells, until the resuspending of the cells after centrifugation. After centrifugation, the pellet was resuspended in bEnd.3-medium with 10 % Dimethyl sulfoxide (DMSO). The volume of one cryovial was 1000 µl medium containing 100 µl DMSO. The cryovials were as fast as possible placed in a cool boy at -20°C. After one day at -20°C, the cryovials were placed in liquid nitrogen for long-time storage and documented in the cryo-documentation on the “Weil-SAMBA”.

2.4 Primary murine neurons preparation

The primary neuronal dissociated cell culture from mice was obtained following the modified protocol from Kaech, Banker, and Moscariello (Kaech and Banker 2006; Moscariello 2018). One day before the preparation, Ibidi dishes (8-well-chamber) and 24-well plates were prepared. The Ibidi dishes were coated with a volume of 200 µl and 24-well plates with 300 µl polyornithine (10 mg/ml, Sigma Aldrich) and Hanks Balanced Salt Solution (HBSS, Gibco) with a concentration of 1:100 and incubated overnight. The HBSS (500 ml) was supplemented with 5 ml Pen/Strep, 3.5 ml HEPES 1M pH 7.25, 1.5 ml Glucose 0.6 %, 5 ml sodium-pyruvate 100 mM. Additionally, the neuronal medium (Neurobasal Medium, Gibco by life technology, Darmstadt, Germany) supplemented with 1mM glutamine (500 µl from 200 mM stock per 50 ml falcon, gibco by life technology) and B27 supplement (1 ml per 50 ml falcon, gibco), was placed into the T75 flask and incubated overnight. Further, the falcon tubes (50 ml), which will contain the brains, were prepared with each 5 ml HBSS (supplemented as described above) and one falcon with 15 ml HBSS. Also, two 50 ml falcon tubes with 70% Ethanol (Roth) were prepared prior.

In the morning before the experiment, the flow hood and the water bath were switched on first. Then the dissection material was put into a plate filled with 70% EtOH. Also, the DNAse I

(500 µl, Roche) was placed on ice. The prior prepared Ibidi dishes and 24-well plates were washed three times with autoclaved water (at least 500 ml). Afterward, the plating medium (2 x 50 ml falcon tubes), which contained MEM, 10% horse serum (5 ml per each 50 ml falcon), and 0.6% glucose (900 µl per 50 ml), was transferred into the wells (200 µl/Ibidi well and 500 µl/ 24-well plate) and stored into the incubator (37°C and 5% CO_2).

Three to four brains were collected from mice pups (P0-1, C57BL/6N). After the brain was removed from the skull, the dissection of the brains underneath the microscope started. At first, the brain was slipped upside down to remove the meninges completely. Following the hindbrain region was separated, and a sagittal cut was performed to separate the two hemispheres. Afterward, the hippocampus, as well as the thalamus, were removed. After that, meninges were entirely removed from the cortex. The cortex was placed into the prior prepared falcon tube with 15 ml HBSS (HBSS 500 ml supplemented with 5 ml Pen/Strep, 3.5 ml HEPES 1M pH 7.25, 1.5 ml Glucose 0.6 %, 5 ml sodium-pyruvate 100 mM) on ice. All prepared brains were collected in the same 15 ml falcon tube.

The tissue was washed three times with 15 ml HBSS (supplemented as above) using a Pasteur pipette and incubated for 20 minutes in a 5 ml aliquot of digestion suspension (trypsin-EDTA) at 37°C. During the incubation time, the tubes were carefully shaken every five minutes. DNAse I subsequently added 5 minutes at room temperature. After three times washing with 5 ml HBSS (supplemented), the tissue was disrupted in 6 ml neuronal plating medium with a standard-sized Pasteur pipette by pipetting it 20 times up and down. Following the tissue was homogenized using a polished Pasteur pipette till the solution is blurred (two times, each one was 20 ups and downs, with a smaller orifice via a fire flame). Subsequently, the suspension was filtered in a sterile 50 ml falcon tube by a cell strainer (40 µm). Following the cells were counted as described below in chapter 2.4. Primary neurons were seeded with cell numbers of 200.000 cells/ 24-well plates and 100.000 cells/ well in Ibidi dish (both materials poly-ornithine coated). After 30 minutes (in the incubator), the plaiting medium was carefully discarded and dropwise replaced with a neuronal medium. Before and after changing the mediums, it was checked if the cells were still attached. Once a week, the medium was exchanged by replacing one-third of the medium with fresh neuronal medium.

Two days after the preparation, the neurons were treated with cytosine arabinofuranoside (araC) (5 µM) to avoid a glial cell cluster. The non-neuronal cells (like glia cells) start to proliferate, and by inhibiting their proliferation, it is possible to yield a “neuron-only” culture (Kaech and Banker 2006; Moscariello 2018).

2.5 Counting of the cells

A cell counter then counted the new passage with 10µl cell suspension and 10 µl tryptophan blue. Trypan-blue is a dye that distinguished between living and dead cells. The hemocytometer and the slip from the cell counter were cleaned with alcohol or bacillol prior. If it was dried, the coverslip was fixed in position. 10 µl of the cell and trypan-blue suspension were added into the hemocytometer (Countess II FL, Invitrogen by Thermo Fisher Scientific). The loading chamber (thick glass microscope slide) was then placed into the hemocytometer. The cell chamber now counted all the cells automatically. It is important to know that the cell calculator gives out a 1:1 dilution per 1 ml.

2.6 Uptake of the nanoparticles

2.6.1 Uptake in bEnd.3 cells

The bEnd.3 cells were seeded with 100.000 cells per well in Ibidi-8-well-chamber. After one day, when the cells were grown confluent, the particles were applied and incubated for 24 hours. The used polymers were polydopamine-Cy5 (PD-Cy5), poly(D-DOPA)-Cy5 (PDD-Cy5), and poly(L-DOPA)-Cy5 (PLD-Cy5). Each particle was applied with a concentration of 50, 100, and 200 µg/ml.

2.6.2 Uptake in neuronal cells

The primary neurons were seeded with 100.000 cells per well in Ibidi-8-well-chamber. The polymers were applied after one week of growth of the neuronal cells, with a well-connected neuronal network, and fixed after 24 hours. The used primary AB were marker soma-neurons (NeuN) and marker astrocytes (GFAP). The used secondary AB were anti-rabbit-Cy3 and anti-mouse-488.

2.7 Fixation of the cells

After the uptake of the polymers (24 h), the cells were washed with PBS buffer three times (at least 200 µl). Afterward, 100 µl of paraformaldehyde (PFA 4%) was added into each well and incubated at room temperature for ten minutes. After the incubation time, the PFA was separately discarded (toxic waste), and the wells were again washed three times with PBS buffer. Also, the PBS was discarded in toxic waste because it could contain some PFA. Following, 200 µl of PBS buffer were left in each well of the Ibidi dish to avoid sample drying.

During the whole fixation process, it was checked underneath the microscope that the cells are still attached.

2.8 Immunocytochemistry

Before cell staining, the wells were washed three times with PBS buffer. Afterward, the samples were blocked and permeabilized with 7% normal donkey serum (Dianova, Hamburg, Germany) with 0.3% Triton (T-8787) in PBS buffer for two hours in the dark at room temperature (RT). Each well contained 100 µl of the blocking solution. Additionally, the Ibidi dish was wrapped in foil to avoid any contact with the light.

After two hours, the samples were washed three times in PBS buffer. If the first antibody was developed, for example in mice, the second one is against mice. The first antibody is called primary anti-body and binds specifically to an antigen. The secondary antibody is coupled to a fluorophore and binds specifically to the primary antibody. The primary antibody was incubated in 2% bovine serum albumin (001-000-161, Hamburg, Germany) and 0.1% (0.3% for organ slices) Triton/ PBS overnight, wrapped in foil in the drawer. The next day, after three washing steps (PBS), the secondary antibody was incubated in 2% bovine serum albumin in PBS for two hours at RT. After the incubation time, the samples were washed three times with PBS buffer. Afterward, DAPI (4',6-diamidino-2-phenylindole, 32670) was incubated for 10 minutes with 0.5 µg/ml. The samples were washed three times with PBS and later embedded in Fluoromout (Biozol, Eching, Germany) to reduce tissue background fluorescence.

Table 1: Primary antibodies used in immunohistochemistry

Name	Cell type	Origin	Concen-tration	Order - number	Company	Storage
GFAP	marker astrocytes	mouse	1: 500	173011	Synaptic Systems	-20 °C
NeuN	marker neurons (soma)	rabbit	1: 500	ABN78	Merck Millipore	4 °C
LAMP1 anti-cluster of differentiation 107a	Lysosome-associated membrane	rat	1:50	553792	Biosciences	4 °C
EEA Anti-early endosome antigen-1	Early endosome antigen	rabbit	1:50	AB50313	Abcam	4 °C

Table 2: Secondary antibodies used in immunohistochemistry

Name	Antigen	Fluorophore Origin	Concen-tration	Order - number	Company	Storage
Anti-mouse IgG	anti-mouse	488 donkey	1: 200	A90-337D2	Bethyl Lab, Biomol	4 °C
Anti-rabbit FAB	anti-rabbit	Cy3 goat	1: 200	711-485-152	Bethyl Lab, Biomol	4 °C
Anti-rat IgG	anti-rat	488 donkey	1: 200	A110-337D2	Bethyl Lab, Biomol	4 °C

2.9 Evaluation of polymers transport across the blood-brain barrier

The transport of the nanoparticles was investigated in transwell assay *in vitro*. The mono-culture with a single layer of bEnd.3 cells on BD Fluoroblok TM Inserts (0.3 cm^2, pore size 3 µm, Corning, Incorporated, Corning, USA) were prepared. Inserts were seeded with 80.00 cells/ insert and placed three days after into the CellZscope device for constant TEER monitoring (400 µl in luminal compartment; 800 µl in abluminal compartment). The polymers were applied luminal with a concentration of 100 µg/ml when TEER values were at least 18-30 Ωcm^2. The transport rate was quantified by the Cy5 label of the used polymers. After 24 h treatment, luminal (1 x 100 µl) and abluminal (3 x 100 µl) medium were transferred in a 96 well-plate. Additionally, fluorescence was measured with TECAN plate reader, and the

percentage of transport was calculated. The transport in percent was measured by using two inserts with cells for each particle and two inserts without cells, which was set to 100 % of transport. The apparent permeability (Papp) was investigated by applying FITC-Dextran 4 (FD4) at a concentration of 100 µg/ml to the luminal side of the transwell system. After 24 hours, the abluminal medium (3 x 100 µL) was collected for FD4 fluorescence measurement. FD4 concentration was determined respectively to a calibration curve obtained by the fluorescence measurement of serial dilutions values. Thus, the apparent BBB permeability coefficient was obtained as following (Artursson et al. 1990; Gaillard et al. 2000).

$$\text{Papp}=\frac{\mathrm{dQ}}{\mathrm{dt}}*\frac{1}{A*C0*60}\ (cm/s)$$

dQ/dt is the amount of transported FITC-dextran per seconds (µg/sec.), A is the surface area of the filter (0.3 cm2), C0 is the initial FITC-dextran concentration (100µg/ml).

2.10 Toxicity Assay on bEnd.3 cell line

The toxicity of polymers and monomers was tested on bEnd.3. Therefore, bEnd.3 cells were seeded on a 96-well plate with 80.000 cells per well. After one day, the polymers (PD, poly(D-DOPA) and poly(L-DOPA) or monomers (dopamine (D), D-DOPA (DD), and L-DOPA (LD) were added with following concentrations 25, 50, 100, 200, 400, and 600 µg/ml in a total volume of 100 µl per well. After 24 hours, 100 µl Cell-Titer-Glo was added per well, shaken for two minutes, and incubated for 10 minutes at room temperature. Afterward, the plate was placed into the luminescent reader. The Cell-Titer-Glo protocol measures each sample three times. The assay reagent measures adenosine triphosphate (ATP) as an indicator of viability and generates a luminescent readout that is much more sensitive than absorbance or fluorescence-based methods (Kijanska, Kelm 2004). All experiments were accomplished in triplicates.

2.11 Toxicity Assay on primary neurons

Additionally, the viability of the polymers and monomers were tested on primary neurons. The neurons were seeded on 24-well plate with 200.000 cells per well. After one week, when the neuron network is fully grown and connected, the polymers were applied (100 µg/ml). Additionally, positive and negative controls were performed. The positive control is one well (on each plate) without any sample, and only neurons medium exchange. The negative control is one well with 1µM staurosporine on the cells (on each plate). Staurosporine induces neuronal apoptosis (Koh et al. 1995). The plates were incubated for 24 hours (37°C and 5% CO_2). After 24 h, cells with the remaining 300 µl medium were incubated with the same volume of Cell-Titer-Glo (300 µl) to reach a total volume of 600 µl. Following the plates were carefully shaken for two minutes and incubated for ten minutes at room temperature. The luminescence reader measured the plates.

2.12 In vitro Parkinson disease model

Further, I have investigated an *in vitro* PD model by introducing neurotoxicity into neuronal cell culture (Laloux et al. 2017). One week after the neuron preparation, when the neuronal network was well developed, I have applied 10 µM 1- methyl-4-phenylpyridinium (MPP^+) and incubated it for 24 h. One day after, I have applied dopamine (D) in different concentrations (0.05, 0.1, and 0.2 µM D) and control (only neurons medium). The plates were incubated for

24 hours (37°C and 5% CO_2). After 24 hours, the viability of the cells was measured with Cell-Titer-Glo and the luminescence reader as prior in 2.10 described.

2.13 Endotoxin Assay

The endotoxin assay was performed following the instructions of the Pierce LAL Chromogenic Endotoxin Quantitation Kit (Pierce LAL Chromogenic Endotoxin Quantitation Kit, 88282). At first, the dilutions for the endotoxin standard stock solutions were performed. The assay was set up by preheating the heating block and equilibrating all substances at room temperature. The samples were diluted to 100, 25, and 10 µg/ml from the stock solution. A neutral pH is needed. At first, a color test was performed to check if the sample significantly interacts with the stop agent (25 % acetic acid). Therefore, 50 µl of the testing sample, 150 µl of endotoxin-free water, and 50 µl of the stop agent were added into one well on a 96-well plate and measured at an absorbance at 405-410 nm, by using the TECAN reader. The assay was performed at 37°C by using 50 µl of the testing sample and 50 µl of the Limulus Amebocyte Lysate (LAL). After 10 minutes of incubation, 100 µl of the chromogenic substrate solution (pre-hated 37°C) was added. It is essential to ensure a homogenous solution and a containing pipetting during the whole experiment. After 6 minutes of incubation, 100 µl of the stop agent was added to each sample. Following the plate was measured using TECAN at an absorbance of 405-410 nm (Brune et al. 2016). Afterward, the average absorbance of the blank replicates was subtracted from the average absorbance of all standards, and samples were calculated to evaluate the mean Δ absorbance. A standard curve by plotting the average blank-corrected absorbance for each standard sample on the y-axis and the corresponding endotoxin concentration in EU/ml on the x-axis was developed. The coefficient of determination, r^2, must be ≥0.98. Following the standard curve (linear regression) was used to calculate the endotoxin concentration of each unknown sample

3 Results

3.1 Culturing of bEnd.3 cells

For cell experiments, it is necessary to check the cells regularly to observe vitality. Cell morphology is one of the most critical points. For example, a slow-growing rate could be a sign of loss of nutrients in the medium (e.g. GlutaMax in DEMEM medium for bEnd.3 cells). Furthermore, it needs to be checked for bacterial contamination. Contamination decreases the vitality of the cells and can be recognized by individual freely moving microorganisms. Even the slightest bacterial contamination leads to the undergo of cells due to the bacteria rapid exponential growth.

In figure 7 is shown, the mouse endothelial cell line (bEnd.3 P19), after two days *in vitro*. In figure 7 b) the cell clusters are getting more confluent and are showing a higher cell number, caused by the division of the cells. During cell division, the volume of the cell is increasing and becomes more rounder. Afterward, the cell nucleus is dividing, and a new membrane is developing in between. The confluence level in figure 7 b) would be estimated at 50-70%. In figure 7 c) is visible, a confluent layer of adherent growing bEnd.3 cells. The “wavy” growing is typical for bEnd.3 cells and reached by 95-100% confluence.

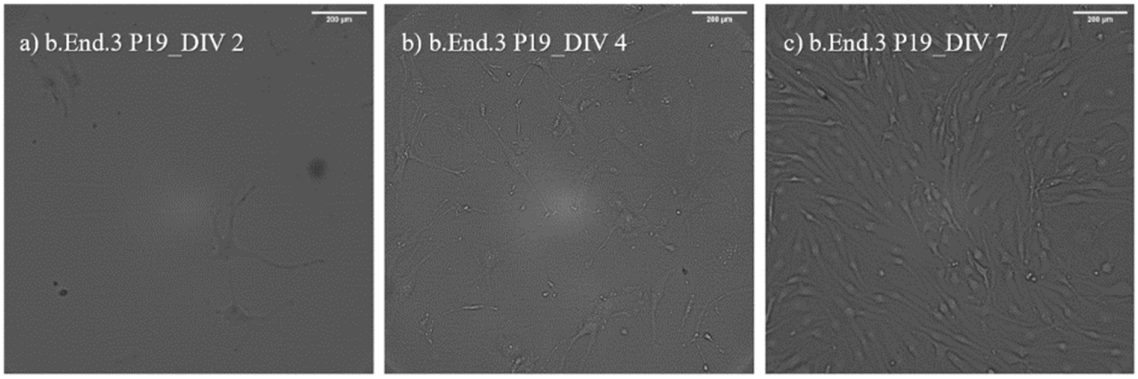

Figure 7: Subcultured adherend b.End.3 cells.
Photos were taken in brightfield by Leica fluorescence microscope (40x), the scale is shown in 200 µm. In this example, the cells were subcultured from passage 18 (P18) into P19. a) Subcultured passage (P19), days in vitro 2 (DIV 2). b) is showing bEnd.3 cells P19 on DIV 4. c) illustrates bEnd.3 cells P19 on DIV 7.

3.2 Culturing murine neuronal cells

For experiments with neuronal cells, it is essential that the neurons develop a network with well-connected neurons. In addition, the viability and the differentiation of the cells were checked. All neuronal cells were grown for at least one week before the experiments. Also, as in 3.1 explained, bacterial contaminations were excluded to guarantee good cell viability.

The cells were prepared and seeded from mice brains after one day of birth. In figure 8 a) is revealed the neuronal cells after one day *in vitro* (DIV 1). After two days, the neurons were treated with cytosine arabinofuranoside (araC) to avoid a glial cell cluster. The non-neuronal cells (like glia cells) start to proliferate, and by inhibiting their proliferation, it is possible to yield a "neuron-enriched" culture. In figure 8 b), the cell development is shown by the increasing growth of the dendrites and axons. In addition, the dendrites are starting to connect. In figure 8 c), a good developed neuronal network is shown. The dendrites and axons were grown in long thread structures and are well connected to each other.

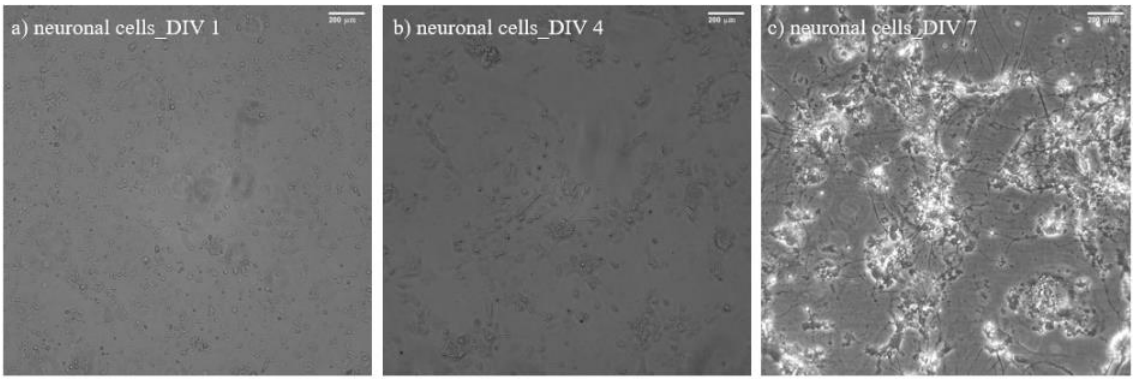

Figure 8: Brightfield pictures of growing neuronal cell culture from mice.
Photos were taken in brightfield by Leica fluorescence microscope (40x), the scale is shown in 200 µm. a) is oberving the single cells one day after the preparation. b) is showing the cells on DIV4. c) is showing the cells on DIV 7, with a neuronal network.

3.3 Cellular uptake of polymer nanoparticles

In physiological conditions, the first barrier from the blood side into the brain side is built by endothelial cells. Therefore, I have analyzed the uptake of the polymers into endothelial cells (bEnd.3) in different concentrations. Following, I have examined the uptake in neuronal cell culture and the uptake into neurons and astrocytes as target cells for the polymer as a possible treatment of PD.

3.3.1 Uptake of polydopamine-Cy5, poly(D-DOPA)-Cy5, poly(L-DOPA)-Cy5 in bEnd.3 cells

The endothelial cell line (bEnd.3) revealed a concentration-related uptake of polydopamine-Cy5 (PD-Cy5) (figure 9). For control cells, without particle uptake, only the nucleus in blue could be observed (figure 9 a). The cells were growing normally, and no background signal for the particle can be visualized. After incubation of 50 µg/ml PD-Cy5, a signal for PD-Cy5 in magenta could be observed in all cells. In figure 9 b), the vesicular uptake (magenta dots) is shown around the blue signal of the cell nucleus. In figure 9 c), a higher signal in magenta and the cytosolic uptake of the particle (particle signal is revealing the morphology of the cell) related to the higher application of 100 µg/ml PD-Cy5 can be observed. The highest signal of the PD-Cy5 particle, also a vesicular and cytosolic uptake, is visible with the highest application of 200 µg/ml (figure 9 d).

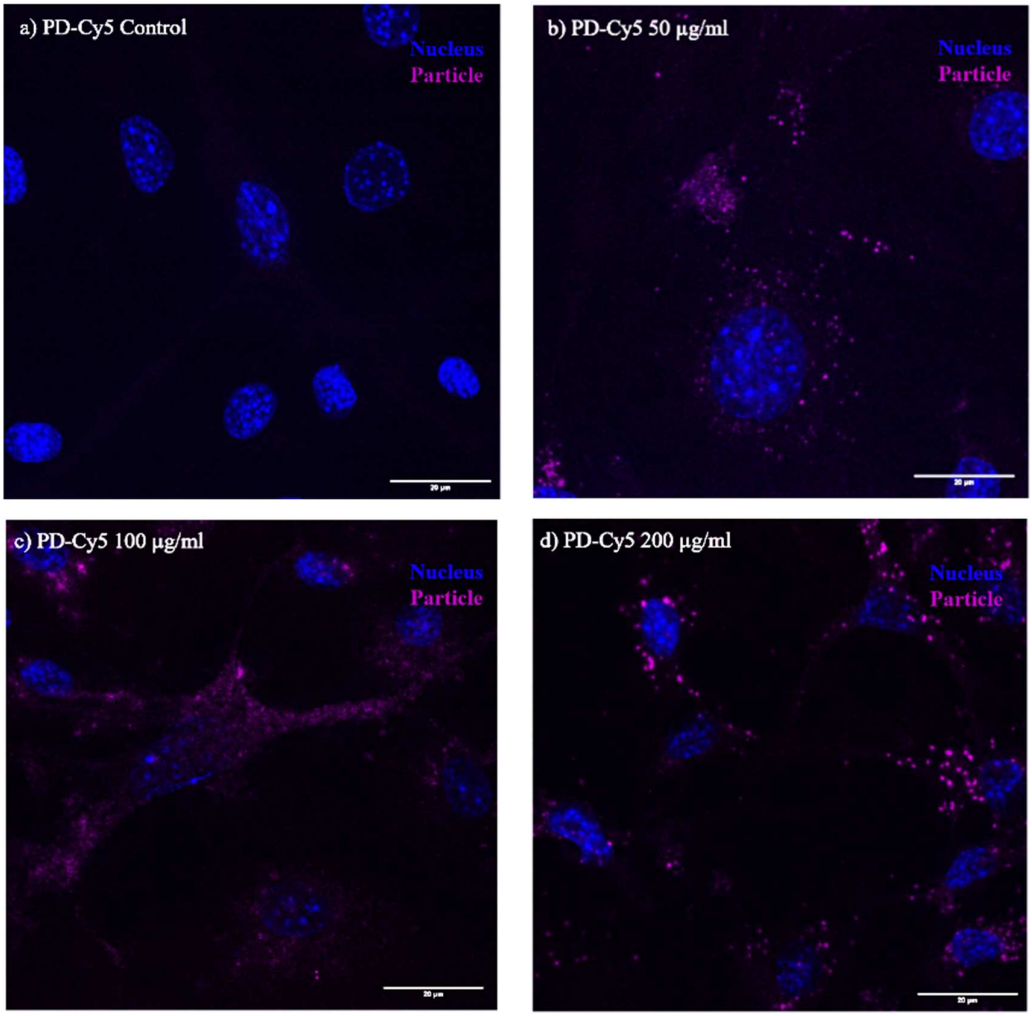

Figure 9: Uptake of polydopamine-Cy5 (PD-Cy5) in bEnd.3 cells.
Confocal images of the endothelial mouse cells (bEnd.3) after 24h incubation with polydopamine-Cy5 (PD-Cy5) in different concentrations. a) control without any particle uptake. b) Uptake of 50 µg/ml PD-Cy5. c) PD-Cy5 uptake with 100 µg/ml. d) 200 µg/ml PD-Cy5. It is shown in blue the DAPI staining, marking the cell nucleus. The particle is visualized in magenta. Scale is 20 µm.

In figure 10 could be observed, the concentration-related uptake of poly(D-DOPA)-Cy5 (PDD-Cy5) in bEnd.3 cells. Figure 10 a) is showing the control. After incubation of 50 µg/ml PDD-Cy5, a signal in magenta in every cell and cytosolic uptake could be visualized (figure 10 b). With increasing concentration of the PDD-Cy5 particle (100 µg/ml), a cytosolic and vesicular uptake in every cell is visible (figure10 c). With the highest application of 200 µg/ml (shown in figure 10 d), a positive signal for the PDD-Cy5 particle (in magenta) in every cell is revealed. Additional to vesicular uptake, a cytosolic uptake could be observed (figure 10 d).

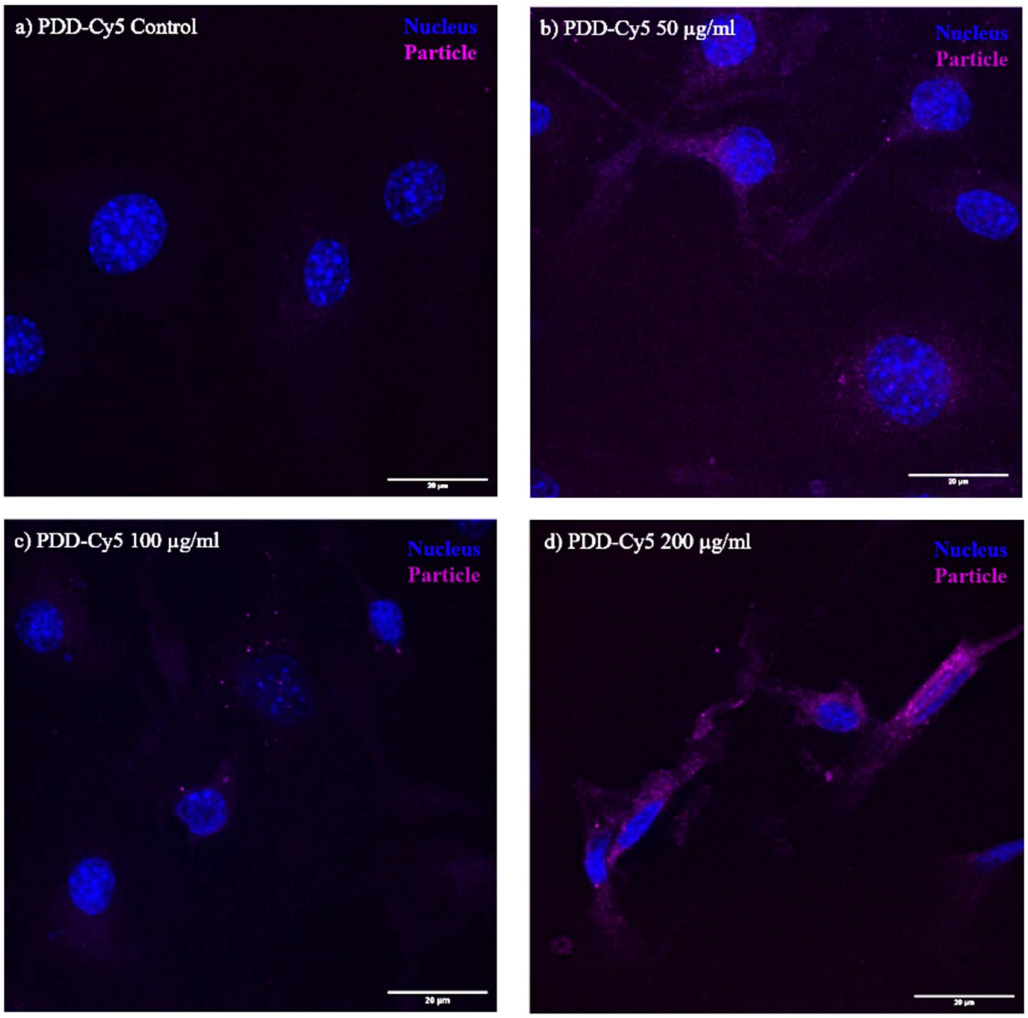

Figure 10: Uptake of poly(D-DOPA)-Cy5 (PDD-Cy5)) in bEnd.3 cells.
Confocal images of the endothelial mouse cells (bEnd.3) after 24h incubation with poly(D-DOPA)-Cy5 (PDD-Cy5) in different concentrations. a) control without any particle uptake. b) Uptake of 50 µg/ml PDD-Cy5. c) Uptake of 100 µg/ml PDD-Cy5. d) Uptake of 200 µg/ml PDD-Cy5. It is shown in blue the DAPI staining, marking the cell nucleus. The particle is visualized in magenta. Scale is 20 µm.

In figure 11 could be observed, a concentration-related uptake of poly(L-DOPA)-Cy5 (PLD-Cy5) in bEnd.3 cells. In figure 11 a) the control is shown. In figure 11 b), after the application of 50 µg/ml of PLD-Cy5, a positive particle signal in magenta in every cell was visualized. In figure 11 c), with a concentration of 100 µg/ml PLD-Cy5, all cells are NP positive (in magenta), and a vesicular and cytosol uptake could be observed. In figure 11 d), with the highest concentration of 200 µg/ml PLD-Cy5, all cells are showing a positive particle signal in magenta. Furthermore, the cytosolic and vesicular uptake can be seen most clear (figure 11 d).

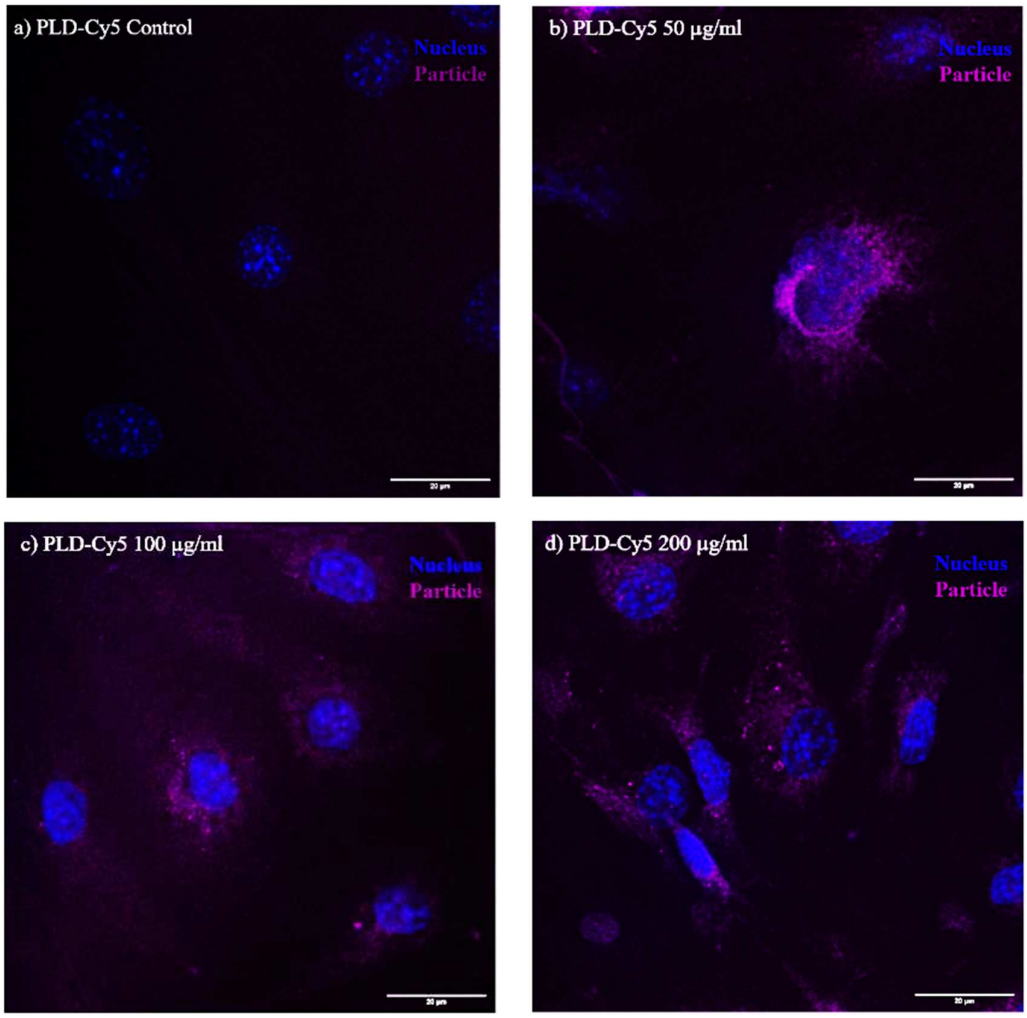

Figure 11: Uptake of poly(L-DOPA)-Cy5 (PLD-Cy5)) in bEnd.3 cells.
Confocal images of the endothelial mouse cells (bEnd.3) after 24h incubation with poly(L-DOPA)-Cy5 (PLD-Cy5) in different concentrations. a) control without any particle uptake. b) Uptake of 50 µg/ml PLD-Cy5. c) Particle uptake with 100 µg/ml. d) Uptake of 200 µg/ml PLD-Cy5. It is shown in blue the DAPI staining, marking the cell nucleus. The particle is visualized in magenta. Scale is 20 µm.

As it is shown above, the polymers are cytosolic and vesicular uptaken in a concentration related manner, into endothelial cells. Therefore, I have investigated the endosomal uptake mechanism of the polymers. Following, I have antibody-stained endothelial cells (bEnd.3) with a marker for early endosomes (EE) and late endosomes (LE).

In figure 12 could be observed, the uptake of polydopamine-Cy5 (PD-Cy5), poly(D-DOPA)-Cy5 (PDD-Cy5), and poly(L-DOPA)-Cy5 (PLD-Cy5) in early and late endosomes in bEnd.3 cells. The controls (figure 12 a) and b) are showing cells without polymers and in blue the DAPI signal of the nucleus. It could be visualized on the left the antibody staining of early endosomes (EE, shown in green), and on the right the antibody staining of late endosomes (LE, shown in green). In the control of figure 12 a) and b), the cells were growing normally, and no background signal for the polymers could be revealed. In figure 12 c) and d), the uptake of 200 µg/ml PD-Cy5 is visible. In figure 12 c), an overlay of the green EE signal and the red signal of the PD-Cy5 particle could be revealed. In figure 12 d), colocalization of the red PD-Cy5 signal and the green signal of the LE antibody staining could be observed. The colocalization of these two signals is indicated by the overlay of the red and green signals in orange, which is also visible in the orthogonal view. In figure 12 e) and f) could be observed, the application of 200 µg/ml PDD-Cy5. Figure 12 e), an overlay of the red particle (PDD-Cy5) and the green EE signals is revealed, further both signals appearing together in the orthogonal view. The PDD-Cy5 signal is also overlapping within the green LE signal (figure 12 f) and visible in the orthogonal view. Figure 12 g) and h) are showing the application of 200 µg/ml PLD-Cy5. In figure 12 g) the red PLD-Cy5 signal and the green EE signals appearing together, demonstrated in the orthogonal view. In figure 12 h), the colocalization of PLD-Cy5 (red) and the green signal of LE appearing together and could be observed in the orthogonal view. Overall, for both stainings (EE and LE), an overlay of the stained cells and the signal for the particle was revealed (figure 12 c, d, e, f, g, and h). It could be visualized that the amount of colocalization of polymer signal in LE is higher compared to polymer signal in EE (figure 12 d, f, and h).

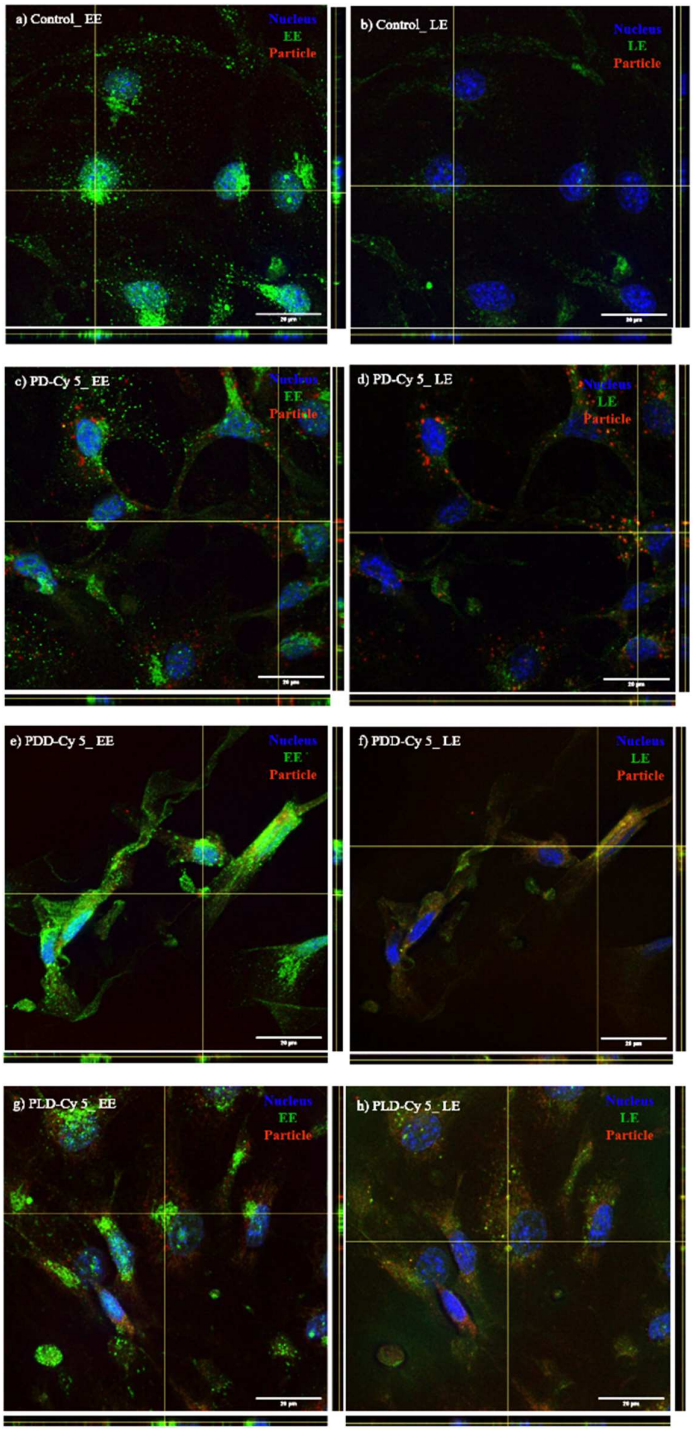

Figure 12: Uptake of 200 µg/ml PD-Cy5, PDD-Cy5, and PLD-Cy5 in early and late endosomes in bEnd.3 cells.

Confocal orthogonal view images of the endothelial mouse cells (bEnd.3), after 24h incubation with polymers. Figure 12 a) and b) are revealing the control, without particle. Figures 12 c) and d) are showing the application of 200 µg/ml of PD-Cy5. Figure 12 e) and f) the application of 200 µg/ml PDD-Cy5. Figure 12 g) and h) Uptake of 200 µg/ml PLD-Cy5. Figures on the left were stained with the antibody for early endosomes (EE in green) (figure 12 a, c, e, and g). The figures on the right were stained with the antibody for late endosomes (LE in green) (figure 12 b, d, f, and h). It is shown in blue the DAPI staining, marking the cell nucleus. All polymers are visualized in red. Scale is 20 µm.

As displayed above, the polymers were uptaken into early and late endosomes of the endothelial cell line (bEnd.3). Higher concentrations of the particle is leading to a higher uptake. To analyze if the polymers are crossing the first barrier from the blood side into the brain side, the transport of the polymers was further investigated (chapter 3.4). Following, I have analyzed the uptake of the polymers into the target cells of the NVU.

3.3.2 Uptake of polydopamine-Cy5, poly(D-DOPA)-Cy5, poly(L-DOPA)-Cy5 in murine neuronal cells

After the polymers showed a positive uptake into endothelial cells (bEnd.3), the polymers were applied to neuronal cell culture to observe an uptake into the target cell of the NVU (neurons and astrocytes).

In figure 13 could be observed the uptake of polydopamine (PD-Cy5) into the murine neuronal cell culture. For control cells, no particle was applied, the cell nucleus in blue is visible (figure 13 a). After incubation of 50 µg/ml PD-Cy5, a signal for PD-Cy5 (in magenta) could be observed in every cell (figure 13 b). In figure 13 c), the magenta signal for the application of 100 µg/ml PD-Cy5 is visible in every cell in the morphology of the neurons. In figure 13 d), with the highest application of 200 µg/ml of PD-Cy5, in every cell the positive particle signal could be observed and visualized the neurons morphology. In figure 13, a concentration-related uptake of the particle (PD-Cy5) could not be observed, in the here used concentrations. The morphology of the NP positive cells indicates an uptake in the target cells of the NVU, which was investigated by antibody staining neurons and astrocytes, shown below in figure 16.

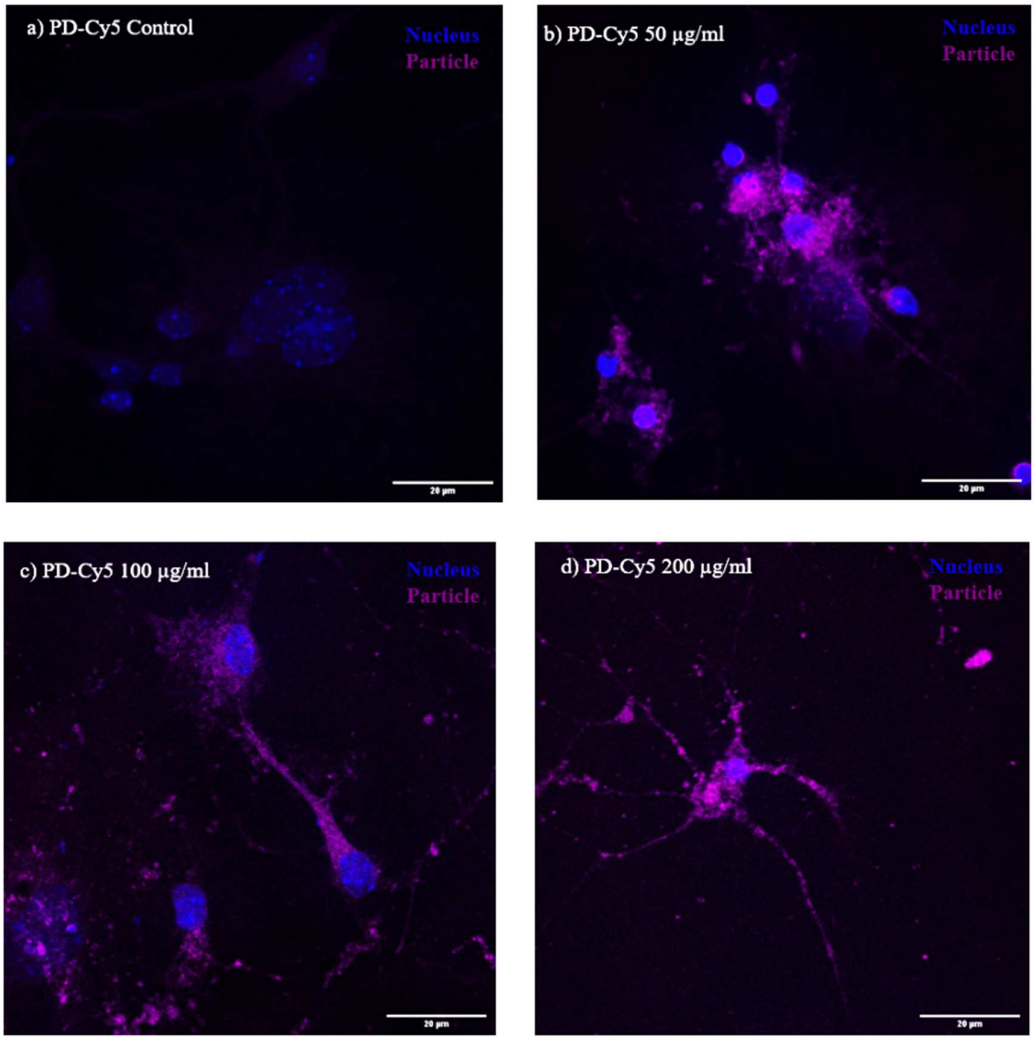

Figure 13: Uptake of polydopamine-Cy5 (PD-Cy5) in neuronal cells
Confocal images of murine neuronal cells after 24h incubation with polydopamine-Cy5 (PD-Cy5) in different concentrations. a) control without any particle uptake. b) Uptake of 50 µg/ml PD-Cy5. c) Uptake with 100 µg/ml in neuronal cells. d) Uptake of 200 µg/ml PD-Cy5. It is shown in blue the DAPI staining, marking the cell nucleus. The particle is visualized in magenta. Scale is 20 µm.

In figure 14, the uptake of poly(D-DOPA)-Cy5 (PDD-Cy5) in murine neuronal cells is visible. After incubation of 50 µg/ml PDD-Cy5, a positive particle signal (in magenta) could be observed in all cells (figure 14 b). Since the positive particle signals are distributed over a large area around the larger cell nuclei, an uptake in astrocytes (large and star-shaped) is assumed. This assumption has been analyzed in figure 17 below. With the application of 100 µg/ml PDD-Cy5, all cells are observing a positive signal for the particle also the morphology of astrocytes and the dendrites of neurons (thread-like particle signal) (figure 14 c). With the application of 200 µg/ml (figure 14 d), all cells are revealing a positive signal for the PDD-Cy5 particle (in magenta), also in the morphology of astrocytes and neurons. A concentration-related uptake of the here applied concentrations of PDD-Cy5 particle could not be observed in figure 14. According to the morphology of the NP-positive cells, the uptake into the target cells of the NVU was analyzed in figure 17.

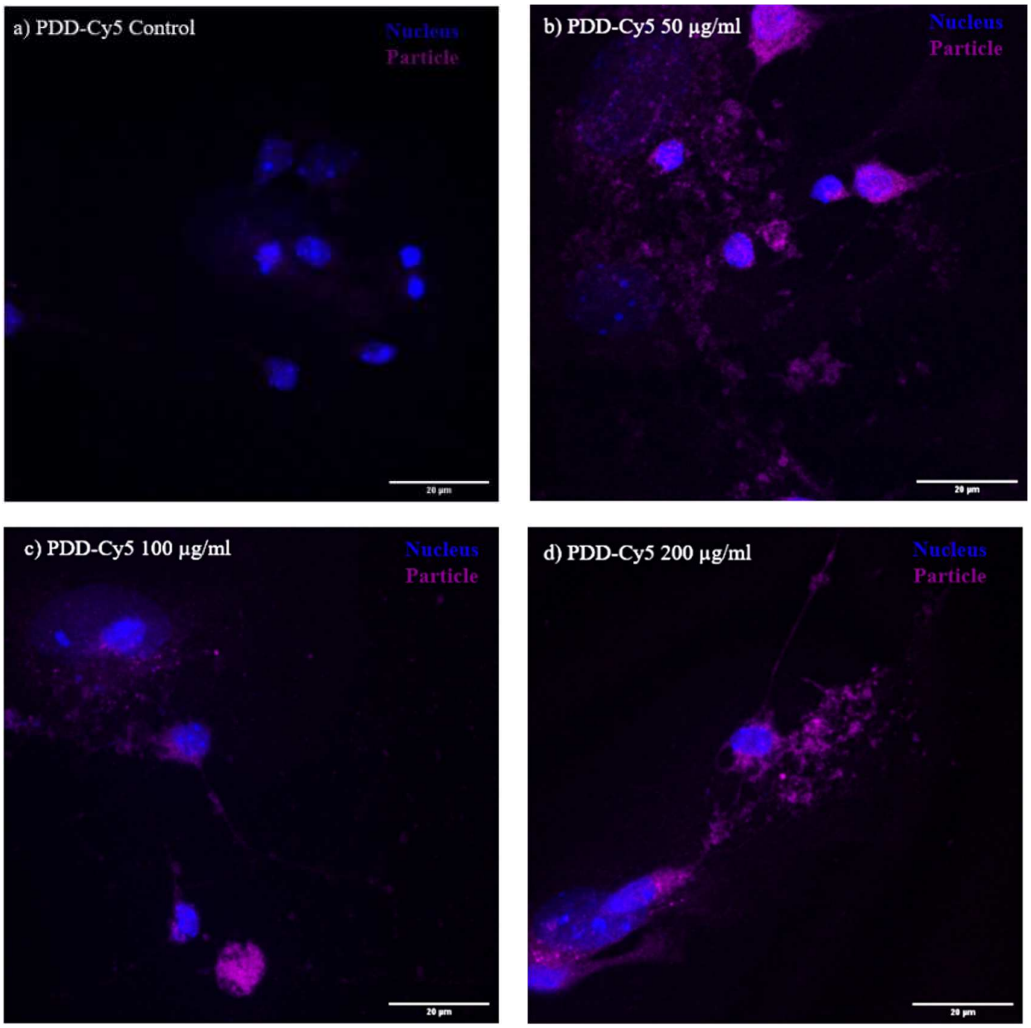

Figure 14: Uptake of poly(D-DOPA)-Cy5 (PDD-Cy5) in neuronal cells.
Confocal images of murine neuronal cells after 24h incubation with PDD-Cy5 in different concentrations. a) control without any particle uptake. b) Uptake of 50 µg/ml PDD-Cy5. c) Uptake with 100 µg/ml. d) Uptake of 200 µg/ml PDD-Cy5. It is shown in blue the DAPI staining, marking the cell nucleus. The particle is visualized in magenta. Scale is 20 µm.

In figure 15, the uptake of poly(L-DOPA)-Cy5 (PLD-Cy5) in murine neuronal cells is visible. After incubation of 50 µg/ml PLD-Cy5, a positive particle signal (in magenta) could be observed in all cells (figure 15 b). Since the positive particle signals are distributed over a large area around the larger cell nuclei, an uptake in astrocytes (large and star-shaped) is assumed. With increasing concentration of the PLD-Cy5 particle (up to 200 µg/ml), no increase of the particle signal in magenta could be observed (figure 15 c and d). According to the morphology of the NP-positive cells, the uptake into the target cells of the NVU was analyzed in figure 18.

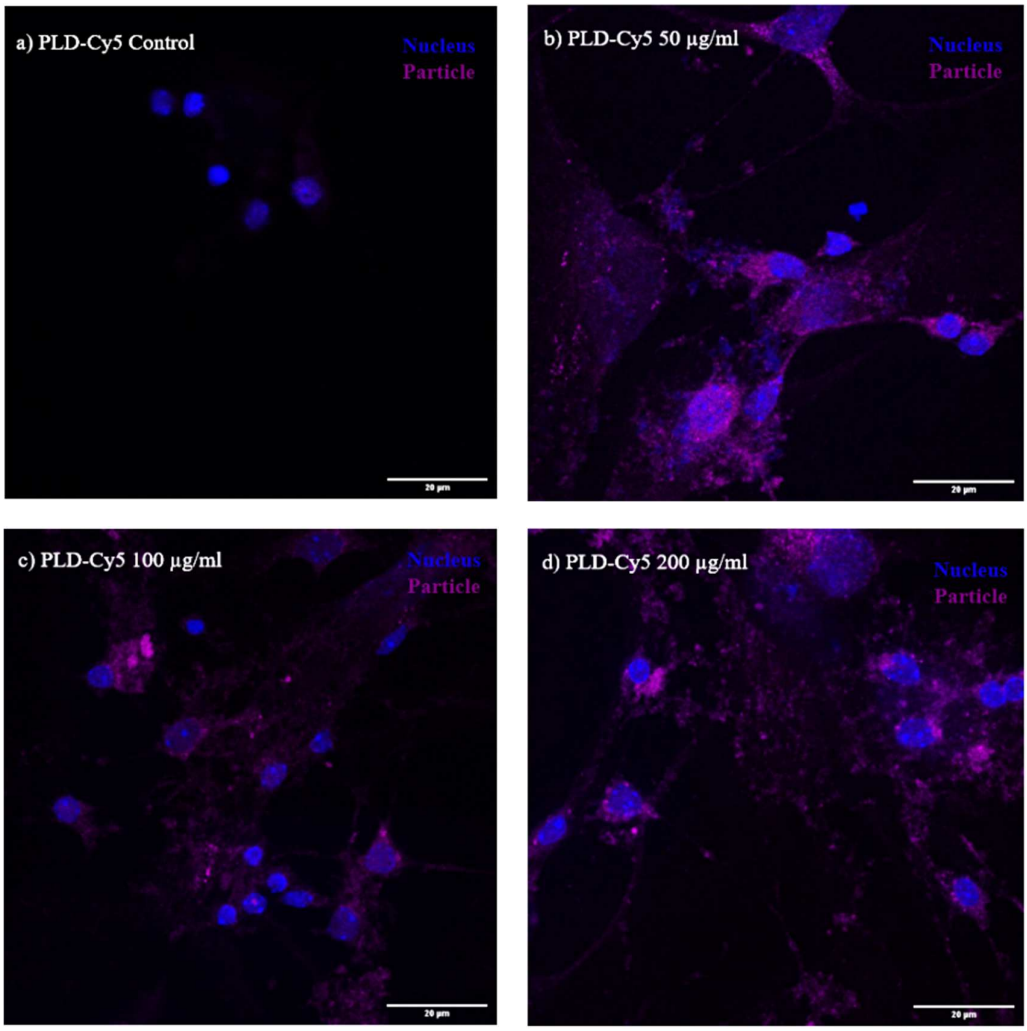

Figure 15: Uptake of poly(L-DOPA)-Cy5 (PLD-Cy5) in neuronal cells.
Confocal images of neuronal cells after 24h incubation with PDD-Cy5 in different concentrations. a) control without any particle uptake. b) Neuronal cells with the uptake of 50 µg/ml PLD-Cy5. c) particle uptake with 100 µg/ml in neuronal cells. d) Uptake of 200 µg/ml PLD-Cy5 in neuronal cells is shown. It is shown in blue the DAPI staining, which marks the cell nucleus. The particle is visualized in magenta. Scale is 20 µm.

In figure 16 could be observed the uptake of the polydopamine-Cy5 (PD-Cy5) particle into neurons and astrocytes. Figure 16 a) is revealing the control without the particle uptake. In figure 16 b) is visible in blue the signal of the nucleus, in green the GFAP antibody staining of the astrocytes, in red the NeuN antibody staining of the neurons, and in magenta the signal of PD-Cy5 particle. After incubation of 50 µg/ml PD-Cy5, a signal for PD-Cy5 (in magenta) could be observed in every cell (figure 16 b). Also, the red neuron signal, green astrocyte signal, and the magenta particle signal are overlapping, which is also shown in the orthogonal view. In figure 16 c) is visible, the application of 100 µg/ml PD-Cy5 and the signals for the nucleus (blue), neurons (red), and astrocytes (green). Again, the particle signal is shown in every cell, and overlapping with the red signal of the neurons and the green signal for the astrocytes, also visible in the orthogonal view. In figure 16 d), the application of 200 µg/ml PD-Cy5 is visible, and the appearing signals of the particle, neurons, and astrocytes.

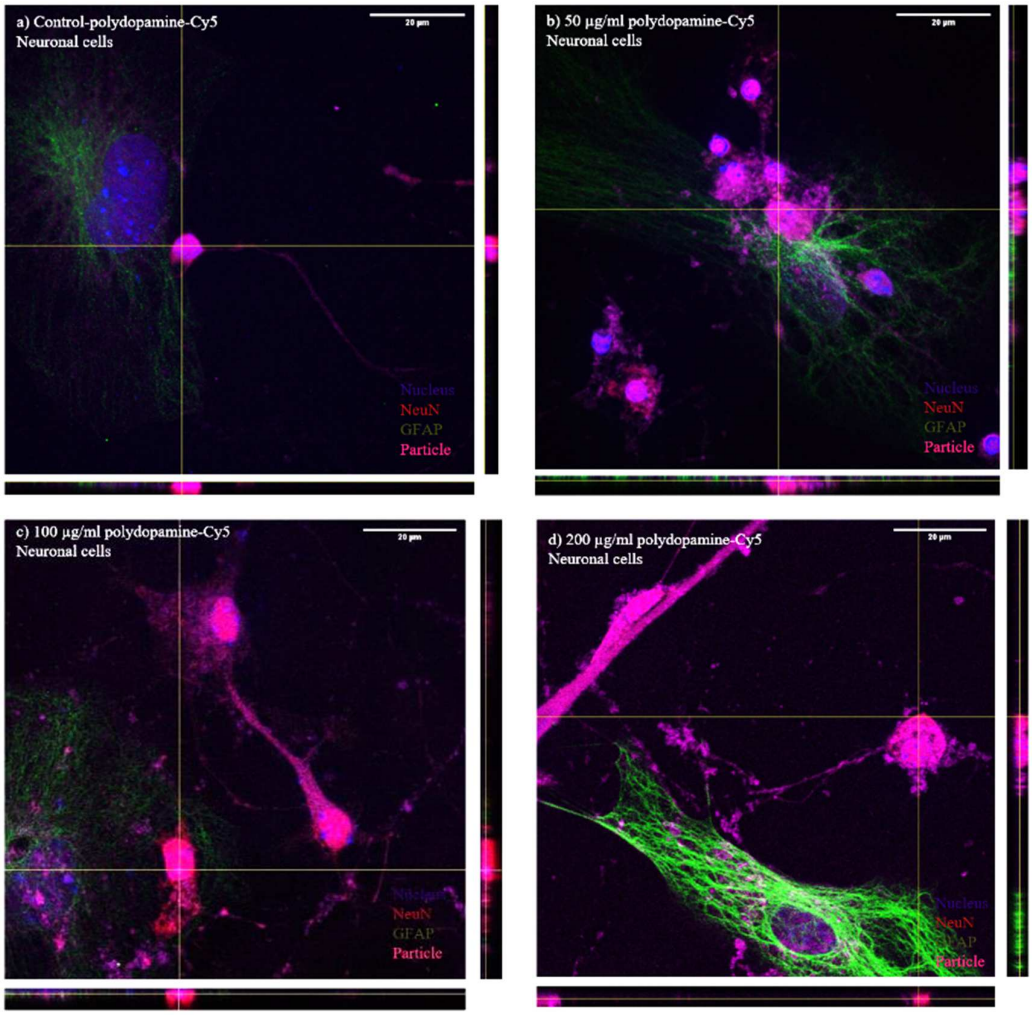

Figure 16: Uptake polydopamine-Cy5 in neuronal cells.
Confocal orthogonal view of primary murine neuronal cells with the uptake of polydopamine-Cy5 (PD-Cy5) in different concentrations. Figure a) Control without particle uptake. Figure b) Uptake of 50 µg/ml of the particle PD-Cy5. Figure c) Uptake of 100 µg/ml and in d) uptake of 200 µg/ml PD-Cy5. All samples were stained with NeuN (red), GFAP (green), and DAPI (blue). Scale is 20 µm.

In figure 17 is shown, the uptake of the poly(D-DOPA)-Cy5 (PDD-Cy5) particle into neurons and astrocytes. In figure 17 a) the control without the particle is visible. In figure 17 b) is visible the nucleus (blue), astrocytes (green), neurons (red), and PDD-Cy5 (magenta). After incubation of 50 µg/ml PDD-Cy5, the particle signal could be observed in every cell (astrocytes and neurons) (figure 17 b). In figure 17 c) could be observed, the application of 100 µg/ml and the colocalization of the red (neurons), green (astrocytes), and the magenta (particle) signals. Also, with the application of 200 µg/ml PDD-Cy5, the particle signal could be observed in neurons and astrocytes (figure 17 d).

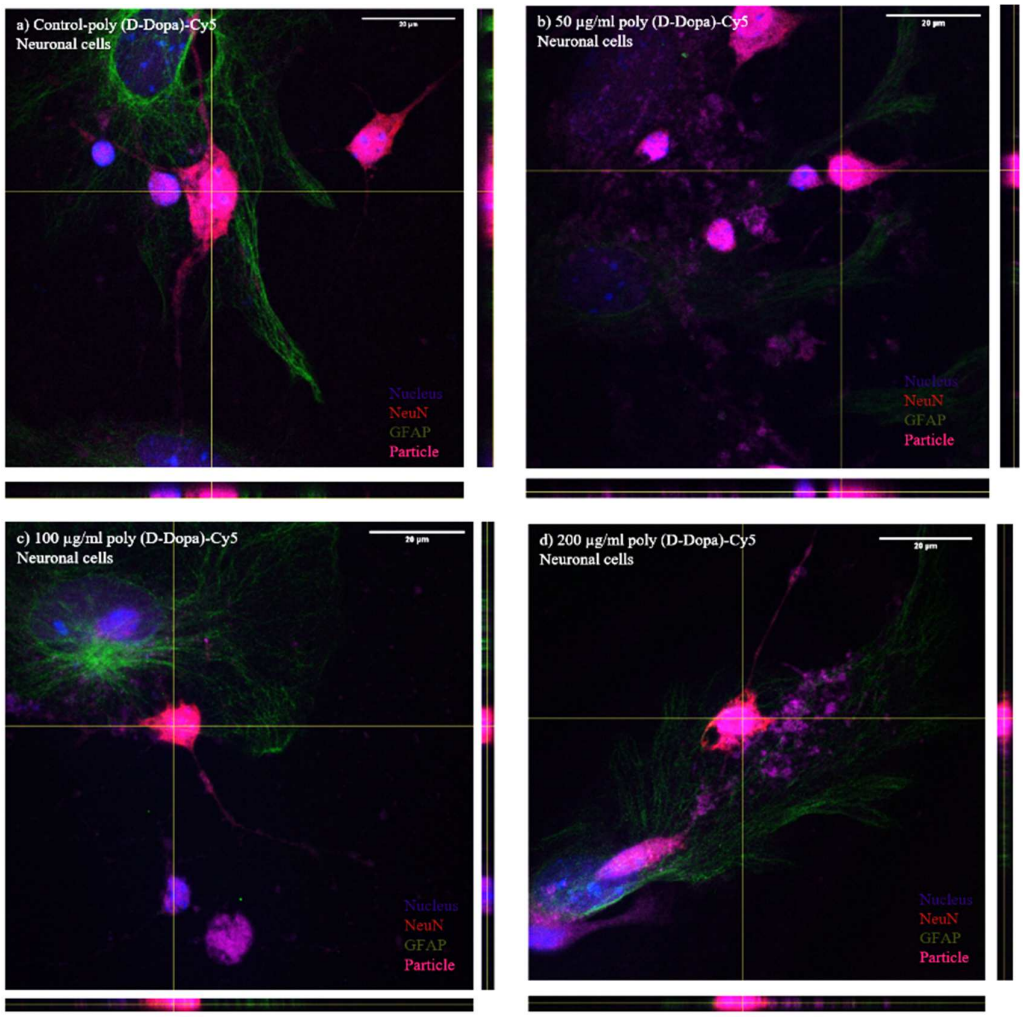

Figure 17: Uptake poly(D-DOPA)-Cy5 in neuronal cells.
Confocal orthogonal view of primary murine neuronal cells with the uptake of poly(D-DOPA)-Cy5 (PDD-Cy5) in different concentrations. Figure a) Control without particle uptake. Figure b) Uptake of 50 µg/ml. Figure c) Uptake of 100 µg/ml and in d) uptake of 200 µg/ml PDD-Cy5. All samples were stained with NeuN (red), GFAP (green), and DAPI (blue). Scale is 20 µm.

In figure 18 could be observed the uptake of the poly(L-DOPA)-Cy5 (PLD-Cy5) particle into neurons and astrocytes. In figure 18 a), the control without the particle is visible. In figure 18 b) is visible the nucleus (blue), astrocytes (green), neurons (red), and PLD-Cy5 (magenta). After incubation of 50 µg/ml PLD-Cy5, the particle signal (in magenta) could be observed in every cell (astrocytes and neurons) (figure 18 b). In figure 18 c) could be observed, the application of 100 µg/ml and the colocalization of the red (neurons), green (astrocytes), and the magenta (particle) signals, visible in the orthogonal view. Also, with the application of 200 µg/ml PLD-Cy5, the particle signal could be observed in neurons and astrocytes in the orthogonal view (figure 18 d).

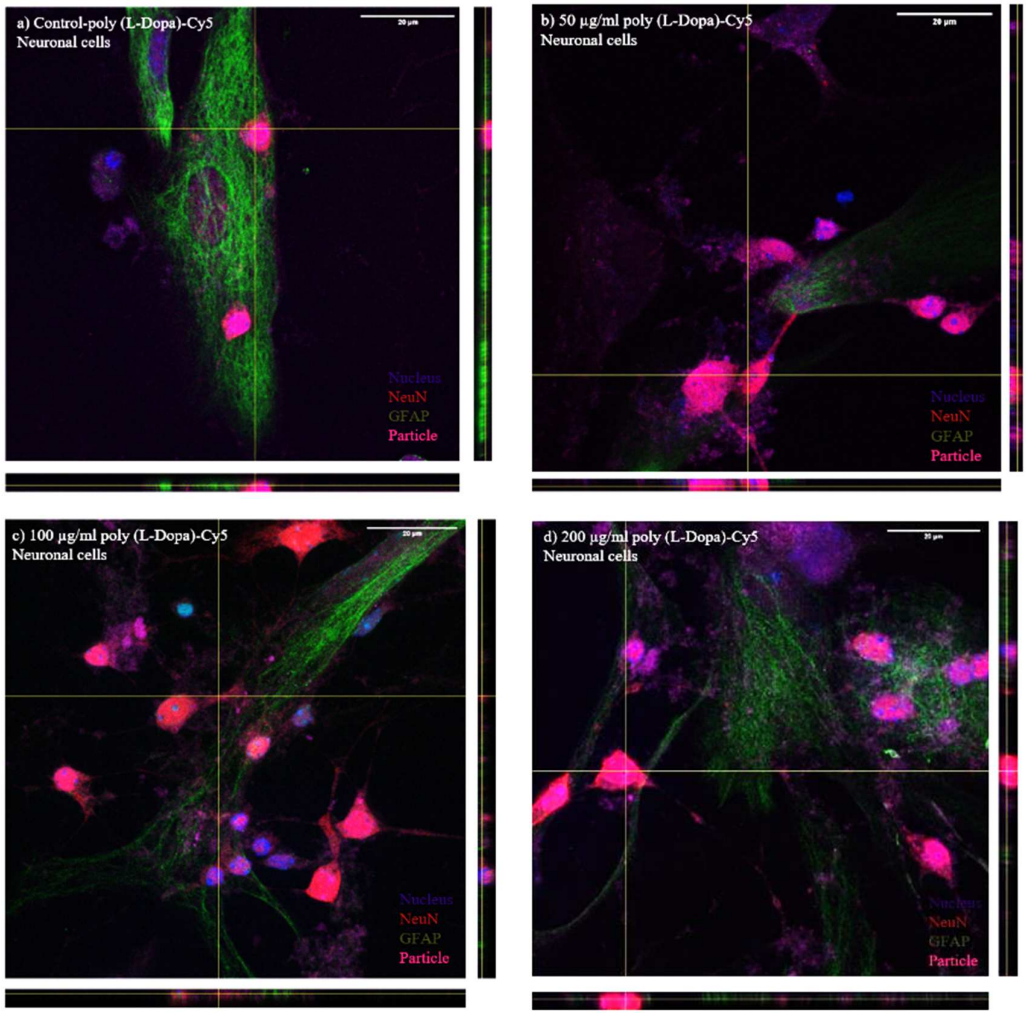

Figure 18: Uptake poly(L-DOPA)-Cy5 in neuronal cells.
Confocal orthogonal view of primary murine neuronal cells with the uptake of poly(L-DOPA)-Cy5 in different concentrations. Figure a) is showing the control of neuronal cells with no particle uptake. Photo b) is showing neuronal cells with the uptake of 50 µg/ml of the particle poly(L-DOPA)-Cy5. In c) the uptake of 100 µg/ml and in d) uptake of 200 µg/ml poly(L-DOPA)-Cy5 in the primary cells are shown. All samples were stained with NeuN (red), GFAP (green), and DAPI (blue). Scale is 20 µm.

3.4 Particle transport across the blood-brain barrier in vitro

In figure 19 could be observed the integrity of the monolayer of endothelial cells (bEnd.3) after the application of the polymers. It is demonstrated the transwell assay with endothelial cells seeded in mono-culture (bEnd.3) (figure 19 a). In figure 19 b, c and d), it is visible the TEER and capacity values are measured by the CellZscope device. Polymers (polydopamine-Cy5, poly(D-DOPA)-Cy5, and poly(L-DOPA)-Cy5) were applied for three independent experiments to the luminal compartment with 100 µg/ml. Per each measurement, the polymers (PD-Cy5, PDD-Cy5, and PLD-Cy5) were analyzed in duplicates and measured independently to visualize the integrity of each barrier. In figure 19 b), the application of the polymers (red line) is visible. Afterward, the TEER is decreasing, and increasing back to the TEER values before applying the polymers. For example, the TEER value for A5 PDD-Cy5 (poly(D-DOPA)-Cy5, in blue) is decreasing from 25 Ωcm^2 before the application, to 34 Ωcm^2 after two hours and is then decreasing to 27 Ωcm^2 (after 10 hours). If the TEER is falling below the initial values, it indicates a leakage of the barrier. If the barrier of the endothelial cells is no longer intact, i.e. the TJs are not closely connected, and the confluent monolayer opens the transendothelial electrical resistance decreases. Furthermore the particle would diffuse paracellular between the opened TJ of the cells, from the luminal into the abluminal compartment.

In figure 19, the TEER (y-axis) scale was set to 100 Ωcm^2, and the scale for the capacity was set to 10 $\mu F/cm^2$. It was possible to set the scales even if the measurements of, for example, control A1 (figure 19 b) is not completely visible in the graph. Because the measurement of control A1 decreases back to the initial values during 4 hours after the particle application and is not falling below the initial value. Also, the capacity of A1 recovers over time. Therefore it can be assumed that the high value is a technical artifact and that the barrier remains intact. Only the TEER measurement of the control C2 is consistently higher after the application and is not recovering during the time. For the experiments in figure 19 c) and d) could be observed that all applied polymers are not falling below their initial values of TEER nor the capacity measurements. All controls were treated with FITC-Dextran 4.

a)

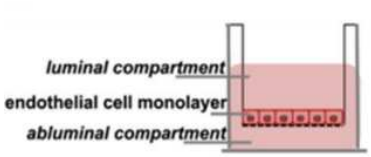
luminal compartment
endothelial cell monolayer
abluminal compartment

b)

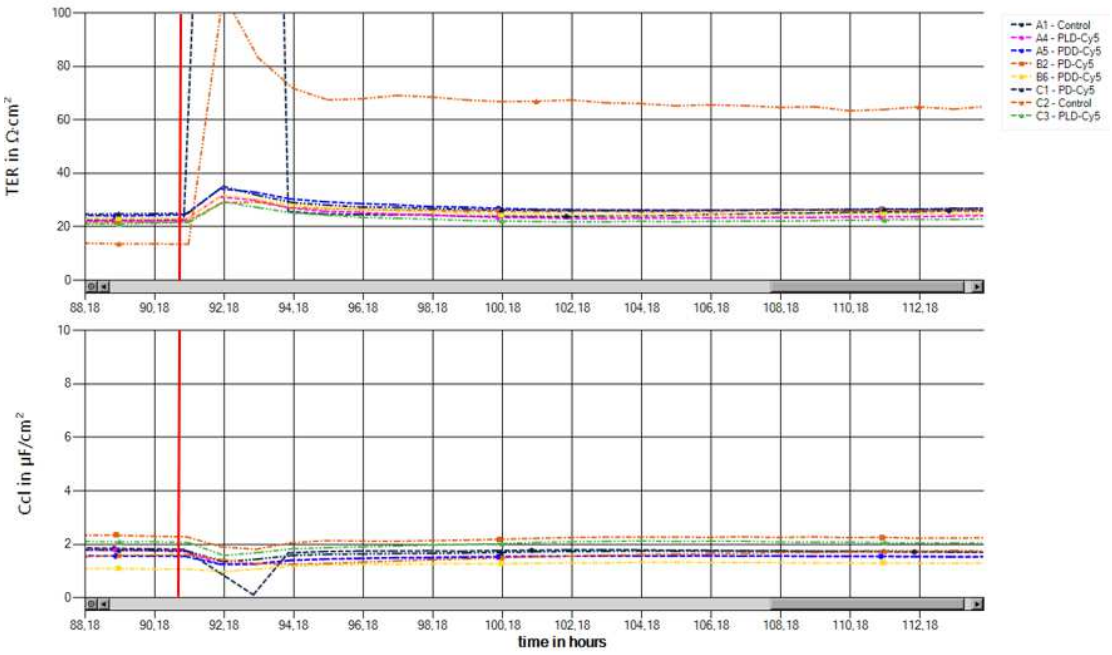
TER in Ω·cm²
Ccl in µF/cm²
time in hours
A1 - Control
A4 - PLD-Cy5
A5 - PDD-Cy5
B2 - PD-Cy5
B6 - PDD-Cy5
C1 - PD-Cy5
C2 - Control
C3 - PLD-Cy5

c)

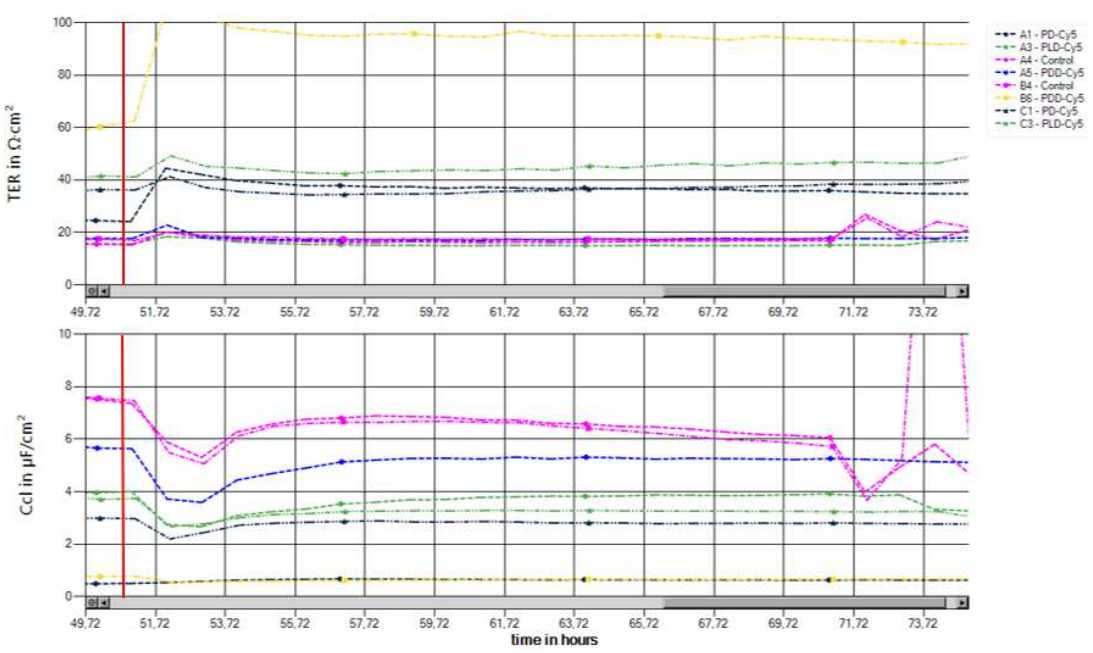
TER in Ω·cm²
Ccl in µF/cm²
time in hours
A1 - PD-Cy5
A3 - PLD-Cy5
A4 - Control
A5 - PDD-Cy5
B4 - Control
B6 - PDD-Cy5
C1 - PD-Cy5
C3 - PLD-Cy5

d)

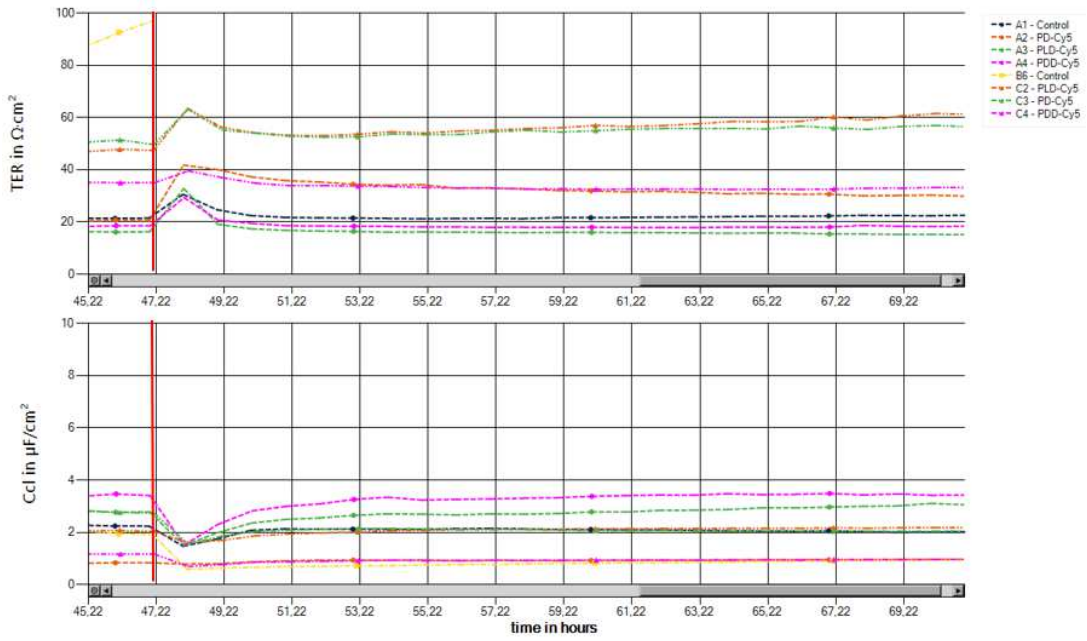

Figure 19: TEER measurement during transport of polymers in vitro.
a) Schematic illustration of transwell setup with endothelial cells seeded in mono-culture (bEnd.3). Figure 19 b, c, and d reveal TEER monitoring (upper graph) and capacity (lower graph) of NPs 3 independent transport assays. TEER and capacity values were determined automatically during the whole experiments by the CellZscope device. Polymers (polydopamine-Cy5, poly(D-DOPA)-Cy5, and poly(L-DOPA)-Cy5) were applied in duplicates to the luminal compartment with 100 µg/ml. The red line is visualizing when the polymers were applied, after 24 h the experiments were stopped.

In figure 20 could be observed, the quantification of the transport of the polymers through an intact barrier of bEnd.3 cells. It is shown polydopamine-Cy5 (PD-Cy5), poly(D-DOPA)-Cy5 (PDD-Cy5), and poly(L-DOPA) (PLD-Cy5) transported from the luminal side to the abluminal side. It could be observed that all polymers have similar high transport capacities, also indicated by the overlapping error bars. The measured transport of PD-Cy5 is 99 ± 23.91 %, PDD-Cy5 is 109 ± 16.29 %, and PLD-Cy5 122 ± 13.42 %.

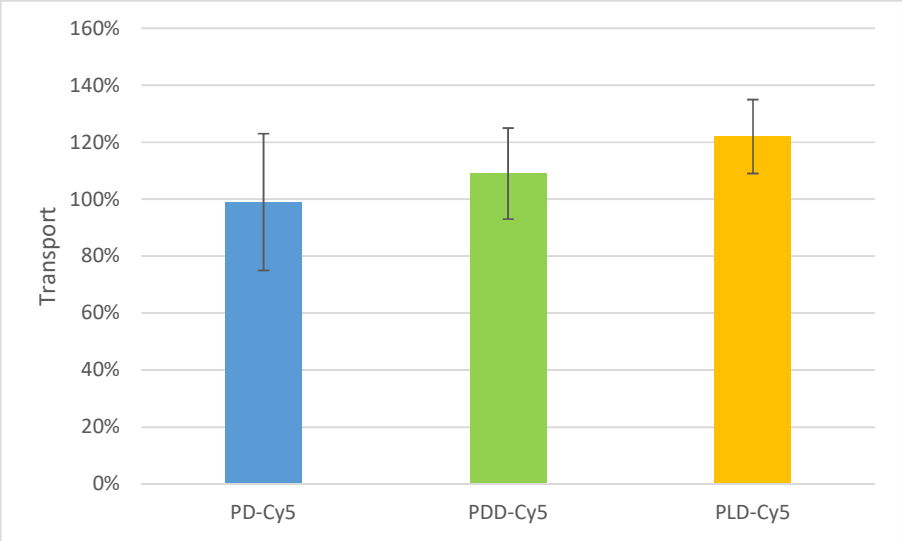

Figure 20: Transport of polymers *in vitro*.
It is demonstrated the transport of the polymers polydopamine-Cy5 (PD-Cy5), poly(D-DOPA)-Cy5 (PDD-Cy5), and poly(L-DOPA) (PLD-Cy5), from the luminal side to the abluminal side, measured by Cy5 fluorescence Data are presented as mean with SD, n = 6 from three independent experiments.

3.5 Toxicity on endothelial cell line

In figure 21 could be observed, the toxicity of the different polymers (PD, PDD, and PLD) to the endothelial cell line bEnd.3. The control (left, in grey) is not treated with any polymer, the viability is set to 100 %. It could be observed the increasing toxicity with a higher concentration of the PDD and PLD polymers. The highest toxicity for the PD polymer was not shown in the highest application (600 µg/ml) but in the second highest of 400 µg/ml. Every sample (PD, PDD, and PLD) reveals the highest viability with the lowest concentration of 25 µg/ml. Also, different toxicities of the various polymers are shown. With a concentration of 25 µg/ml PLD (orange) shows the highest viability (138 ± 4%) compared to PD (116 ± 10 %, blue) and PDD (90 ± 3 %, green). Overall, it is clearly shown, the viability is depending on the concentration of the polymers.

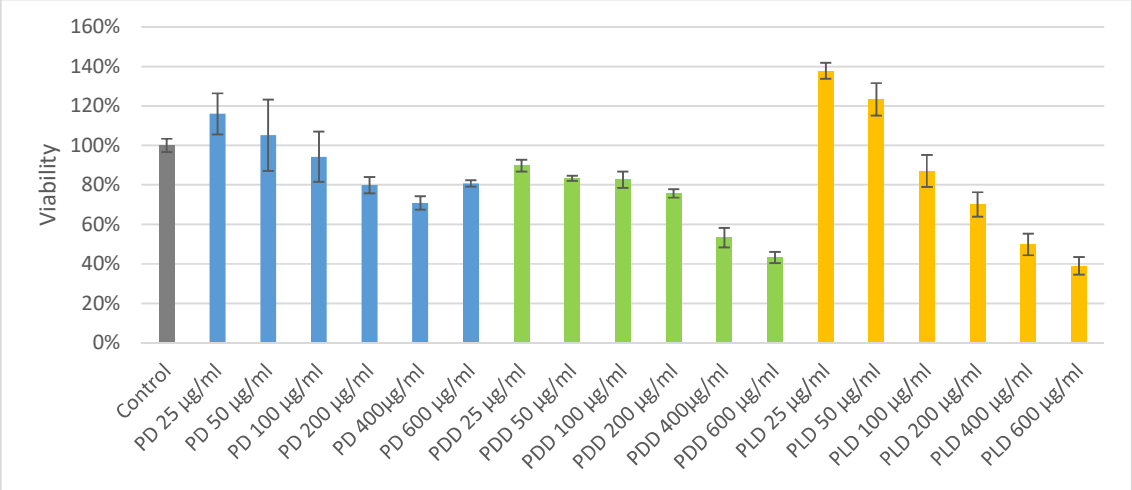

Figure 21: Toxicity of polymers on b.End.3 cells.
Viability in percent, depending on the concentration of the polymers of 25, 50, 100, 200, 400, and 600 µg/ml after 24 h incubation. Polydopamine (PD, blue), poly(D-DOPA) (PDD, green), and poly(L-DOPA) (PLD, orange) are shown. The medium control is shown in grey. Data are presented as mean with SD n = 3 from one experiment.

In figure 22 could be revealed, the toxicity of the different monomers (D, DD, and LD) to the endothelial cell line bEnd.3. The control (left, in grey) is not treated with any particle, the viability is set to 100 %. In every sample is shown, the increasing toxicity with a higher concentration of the monomer. Otherwise, decreasing viability with increasing concentration is recognized. Every sample (D, DD, and LD) shows the highest viability with the lowest concentration of 25 µg/ml. Also, different toxicities of the various monomers are shown. With a concentration of 25 µg/ml LD (orange) shows the highest viability (99 ± 3 %) compared to D (88 ± 4 %) and DD (46 ± 1 %). With a 600 µg/ml concentration, the viability is the lowest for every sample. The lowest viability of LD is 10 ± 0 % and for DD and D 0 ± 0 %. Overall, it is clearly shown, the concentration related viability of the monomers.

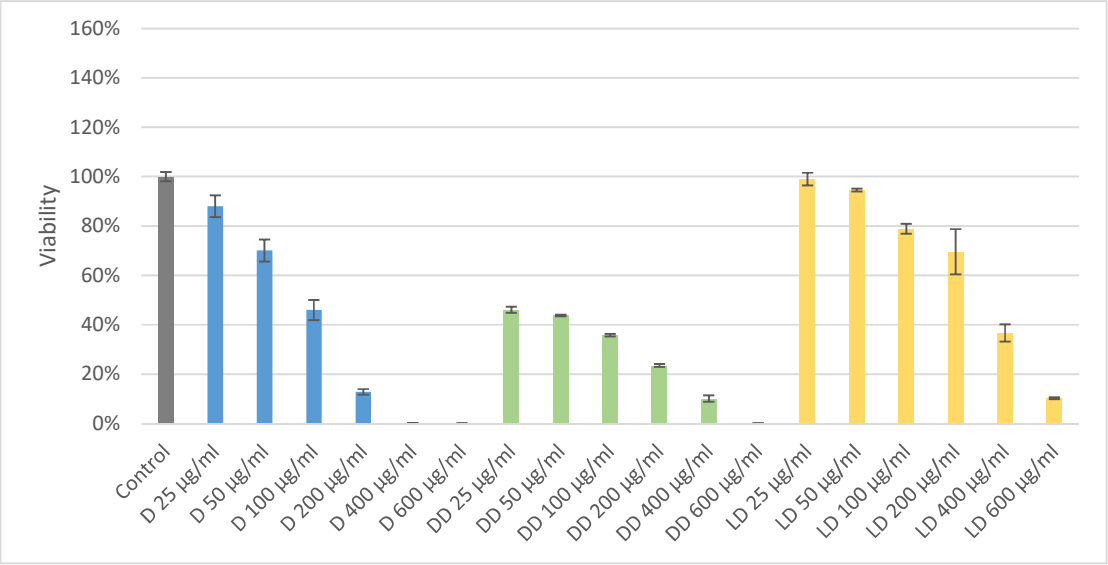

Figure 22: Toxicity of monomers on b.End.3 cells.
Viability in percent, depending on the concentration of the monomers of 25, 50, 100, 200, 400, and 600 µg/ml after 24 h incubation. It is shown dopamine (D, light blue), D-DOPA (DD, light green), and L-DOPA (LD, light orange). The control is shown in grey. Data are presented as mean with SD, n = 3 from one experiment.

3.6 Neurotoxicity of polymer and monomer particles

In figure 23 is visualized the toxicity of the polymers (PD, PDD and PLD) and monomers (D, DD, and LD) to neuronal cell culture. The control (left, in gray) is medium and set to 100 percent, with a viability of 100 ± 6 %. The polymer concentration (100 µg/ml) equals the monomer concentration (40 µg/ml) because the polymers is built by 40 % polymerized monomer and 60 % PEG. It is observed, the higher toxicity from DD and LD monomers compared to PDD and PLD polymers. Due to the overlapping error bars between PD and D, no differences of the viability could be observed. All polymers show similar viabilities or toxicities (PD 52 ± 4 %, PDD 48 ± 1 %, and PLD 48 ± 6 %). The toxicity of DD is the highest (viability of 22 ± 4 %), compared to D (viability of 35 ± 16 %) and LD (viability of 31 ± 5 %). Staurosporine (left, in black) is showing the negative control and reveals the highest toxicity and the lowest viability with 12 ± 1 %.

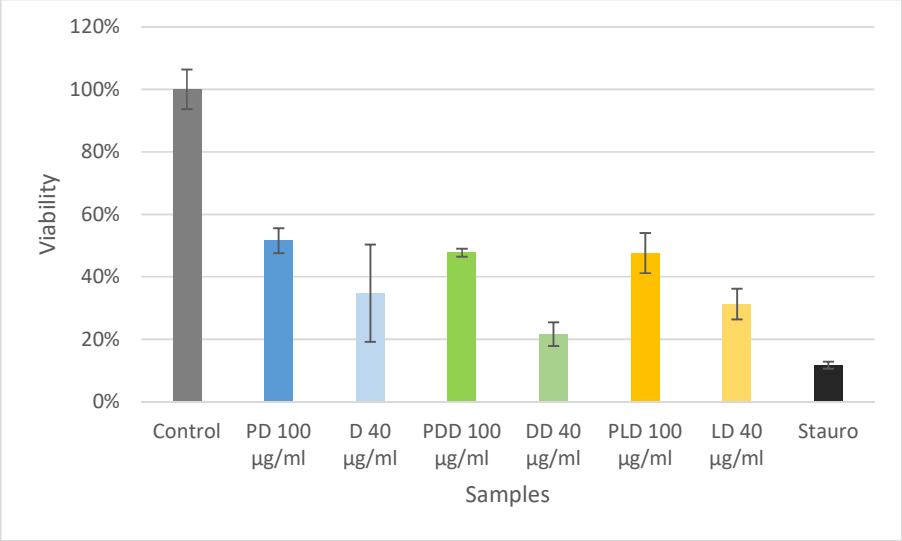

Figure 23: Neurotoxicity of monomers and polymers on neuronal cell culture.
It is shown the viability of the different samples on neuronal cells. All monomers are shown in a concentration of 40 µg/ml, and all polymers are shown in a concentration of 100 µg/ml. The polymers are built of 40 µg/ml polymerized monomer and 60 µg/ml PEG. It is shown from left to right, the control (grey), polydopamine (PD, blue), dopamine (D, light blue), poly(D-DOPA) (PDD, green), D-DOPA (DD, light green), poly(L-DOPA) (PLD, orange), L-DOPA (LD, light orange) and staurosporine (stauro, black). Data are presented as mean with SD, n = 3 from one experiment.

In figure 24 is shown the toxicity of a three-month-old batch of polymers (PD, PDD and PLD) to neuronal cell culture. During experiments, a variation of the viability of the polymer samples was visible. Therefore, a three-month-old polymer batch was applied to neuronal cells to analyze the toxicity. Higher toxicity of the old polymers (figure 24) could be observed. With a concentration of 100 µg/ml on the cells, all samples viability is below 50 %. For PD the viability is 41 ± 3 %, PDD 23 ± 4 %, and PLD 33 ± 9 %. The control (left, in grey) is treated with medium and set to 100%, the viability is 100 ± 11 %. Staurosporine (right, black) is showing the highest toxicity and the lowest viability of 14 ± 0 %.

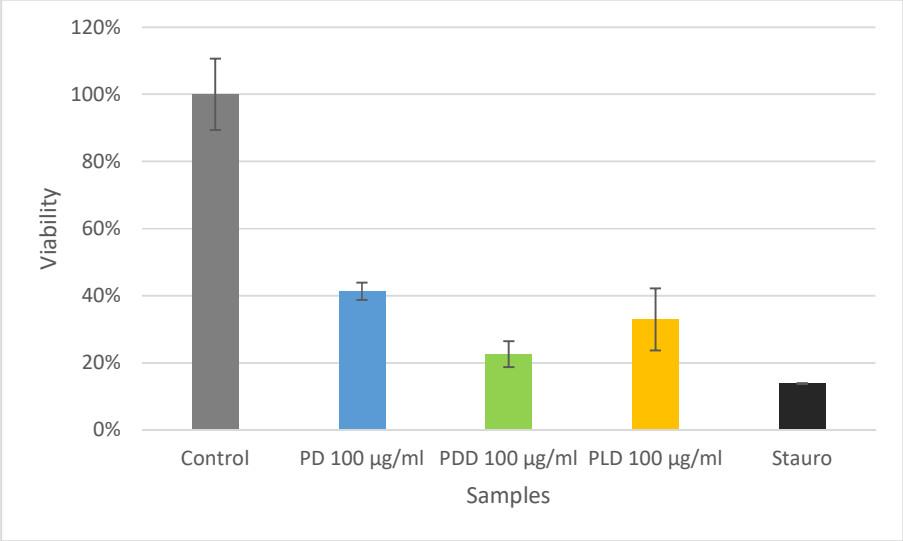

Figure 24: Neurotoxicity of a three-month-old batch of polymers on neuronal cell culture.
It is shown, the viability of neuronal cells, depending on different three-month-old samples. It is shown from left to right, the control (grey), polydopamine (PD, blue, 100 µg/ml), poly(D-DOPA) (PDD, green, 100 µg/ml), poly(L-DOPA) (PLD, orange, 100 µg/ml), and staurosporine (stauro, black). Data are presented as mean with SD, n = 3 from one experiment

3.7 Endotoxin load of polymer and monomer particles

After the older polymers neurotoxicity assay has shown higher toxicity, the endotoxicity was analyzed. All samples have been sterile filtered (20µm) after synthesis before applying them to the cells. It is crucial to sterilize the polymer batches right after the synthesis to avoid any bacterial growth. A bacterial contamination after polymer application on the neurons was not observed. Therefore, I have analyzed the samples of endotoxin contamination. Endotoxins are released from gram-negative bacteria (before sterile filtration). The sterile filter will not filter the endotoxins.

In table 3, the endotoxin pollution of the polymers could be observed. The lower endotoxin pollution of the unlabeled samples (PD, PDD, and PLD) is visible. Otherwise, the higher endotoxin burden of the Cy5 labeled samples is indicated (PD-Cy5, PDD-Cy5, and PLD-Cy5).

Table 3: Endotoxin units per ml (EU/ml) for different NP samples.
Results have been determined by "Pierce LAL Chromogenic Endotoxin Quantitation Kit (88282)"

NP sample (100 µg/ml)	Endotoxin Unit per 100 µg/ml
Polydopamine (PD)	3.5844
Polydopamine-Cy5 (PD-Cy5)	24.054
Poly(D-DOPA) (PDD)	0.7880
Poly(D-DOPA)-Cy5 (PDD-Cy5)	2.3176
Poly(L-DOPA) (PLD)	0.9064
Poly(L-DOPA)-Cy5 (PLD-Cy5)	1.8644

3.8 Dopamine-related rescue of *in vitro* Parkinson disease model

It is shown the *in vitro* PD model (figure 25) with the application of dopamine in different concentrations. The cells were 24 h prior perpetrated with the chemical 1-methyl-4-phenylpyridinium (MPP^+, 10 µM). MPP^+ is introducing neurotoxicity on neuronal cells and is therefore used as an *in vitro* PD model. The dopamine was applied in different concentrations (00.5, 0.1, and 0.2 µM). The control in grey on the left side was not treated with MPP^+ and the set to 100%. The medium MPP^+ sample was treated with the chemical (MPP^+), and only medium was applied and no dopamine. It is shown a difference of the viability between the untreated neuronal cells (control, in dark grey) and the MPP^+ treated cells with medium (Medium MPP^+, in light grey). The viability of the control is at 100 ± 18 %, and the viability of the Medium MPP^+ sample is 21 ± 3 %. Besides, it is shown a dopamine concentration-related rescue of the neuronal cells. The higher dopamine concentration (0.2 µM) is showing the highest viability of the neuronal cells 49 ± 9 %. With increasing dopamine concentration, the viability is increasing from 19 ± 5 % (0.05 µM D) to 26 ± 2 % (o.1 µM D).

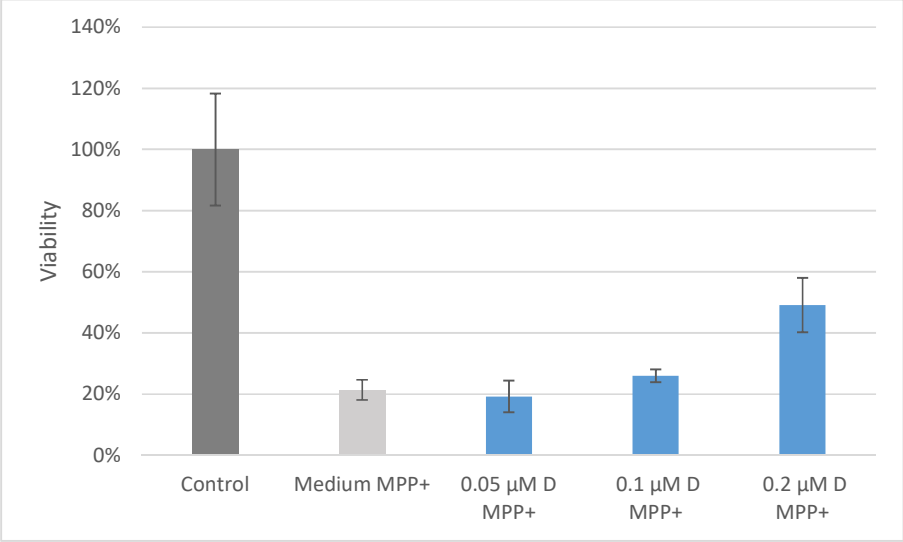

Figure 25: Dopamine-related rescue of *in vitro* PD Model on neuronal cell culture.
It is shown the viability of neuronal cells after MPP^+ (10 µM) treatment for 24 h depending on the concentration of dopamine (incubation 24 h). It is shown from left to right, the control with medium (dark grey), the MPP+ treated neuronal cells with medium treatment (light grey), the MPP+ treated cells with 0.05 µM dopamine (blue) treatment, MPP+ cells with 0.1 µM dopamine (blue) treatment, and MPP+ cells with 0.2 µM dopamine (blue) treatment. Data are presented as mean with SD, n = 3 from one experiment

4 Discussion

Caused by the increasing impact of neurological diseases on public health, the need of a non-invasive method to better treat the patients is more evident than ever (WHO 2006). Neurological disorders are closely linked to the physiology of the neurovascular unit (NVU) in the brain. The NVU incorporates three main functionalities, the blood-brain barrier (BBB), neuroimmune axis, and regulation of the cerebral blood flow (Neuwelt et al. 2011). Therefore, nanoparticles have been investigated for testing potential drug penetration to the central nervous system across an intact BBB (Vong et al. 2020). Currently used methods are often invasive and having a high potential for negative side effects, and are less efficient (B. Sampaio-Maia et al.; Cheng et al. 2010; Meiser 2013). According to the need for better treatment, I have analyzed polymers, which could be promising as a further treatment for neurological diseases, for example, Parkinsons disease.

4.1 Cell uptake and transport across an intact barrier of the polymers

For this thesis, customized polymers for further drug delivery of therapeutic agents into CNS were designed and prepared by Dr. Sean Harvey from the laboratory of Prof. Tanja Weil at the Max-Planck Institute for polymer research in Mainz. These polymers were composed of polymerized dopamine, D-DOPA, and L-DOPA with the crosslinked copolymer polyethylene glycol (PEG 3000), with a size less than 50 nm (Harvey et al. 2018). To investigate the ability of the newly developed polymers as a potential neurological treatments for example in Parkinson disease, by replacing dopamine in the brain to support the undergoing dopaminergic neurons.

The blood-brain barrier separates the blood from the brain side, and the capillary of these blood vessels is built on the inner side of endothelial cells (Abbott 1986). Therefore in physiological conditions, the endothelial cells (luminal side) must be penetrated at first to overcome the barrier and reach the brain parenchyma (abluminal side) (Abbott 2003; Mikitsh and Chacko 2014). Therefore, in the very first beginning, I have analyzed the uptake of these polymers into endothelial cells. By analyzing confocal images of the endothelial cell line bEnd.3 with polymers uptake (after 24 h incubation), uptake of the polymer (magenta) into the cells, and the cell nucleus (blue) could be observed (figures 9, 10, and 11). In figure 9), a concentration-related uptake of the polymers polydopamine-Cy5 (PD-Cy5) could be perceived. In figure 10), the concentration-related uptake of poly(D-DOPA)-Cy5 (PDD-Cy5) is visible, and in figure

11), the concentration-related uptake of the poly(L-DOPA)-Cy5 (PLD-Cy5) polymer is detected. Each polymer showed a higher uptake into bEnd.3 cells with increasing polymer concentration (from 50 µg/ml up to 200 µg/ml). Differences in uptake of the respective polymers (PD-Cy5, PDD-Cy5, and PLD-Cy5) could not be observed. Further, the intensities between the polymer signals should not be compared, caused by different fluorescence intensities within the respective samples and therefore cannot be compared quantitatively.

Caused by the tighter coupled intercellular junctions (tight junctions) of the brain endothelial cells (BECs), which significantly reduce the permeation of ions and large hydrophilic solutes through the intercellular cleft via the paracellular pathway, the polymers needs a pathway to overcome the barrier (Neuwelt et al. 2011; Keller 2013). Therefore, essential molecular delivery has to use vesicular pathways. The transport way of the receptor (specific)- and adsorptive (unspecific) -mediated transcytosis is responsible for the regulated vesicular transport of larger molecules, including peptides, proteins, and large pharmaceutical drugs (Toth et al. 2019). In addition, the figures (9, 10, and 11) are indicating the uptake of the polymers into the cytosol (cloudy intracellular signal) and vesicles (round strong intracellular signals) in endothelial cells. The complex vesicular transport machinery involves a diverse set of vesicular entities such as early, late, and recycling endosomes, exosomes, ectosomes, retromer-coated vesicles, lysosomes, trans-endothelial channels, and tubules (Toth et al. 2019). Therefore, intracellular trafficking was further investigated by antibody staining with a marker for early and late endosomes, shown in figure 12. The antibody staining supports the thesis of the endosomal transportation of the polymers by overlaying signals in confocal images. It could be observed, an overlay of the polymer in magenta in the early endosomes (EE, green) in figure 12 c, e, and g. Additionally, colocalization of the polymer signal in late endosomes (LE, green) could be visualized in figure 12 d, f, and h.
The central sorting station in the endocytotic pathway are the early endosomes by receiving receptors and cargos from almost all endocytotic uptaken vesicles (Toth et al. 2019). The early endosomes enter into the process of endosomal maturation and mature into late endosomes, and some of them into lysosomes (Toth et al. 2019).

In figure 12 the signal of the polymers in the early endosome is indicating that the polymers are endocytosed. Further, the signal in the late endosomes could come from the maturated early endosomes, or for example, from the cytosol. After the polymer is endocytosed from EE, it could be released into the cytosol and then uptaken into late endosomes. Additionally, it is

hypothesized that the long incubation period of 24 h is leading to a higher signal of the polymer in late endosomes. Moreover, vesicles that are neither EE or LE showed a positive polymer signal. The assessment which can be done after analyzing figure 12 is that the polymer is endocytosed into early endosomes, is visible in late endosomes, unknown vesicles, and is also shown in the cytosol. Indicating a possible transcytotic trafficking of the particle. An endocytosis on the luminal side of the endothelial cells, a trafficking through the cell, and a release on the abluminal side of the cell should addressed in future studies. The polymer for example could not be not exocytosed on the abluminal side and instead be released on the luminal side or ending in lysosomal degradation. It is known that the lysosomal degradation is challenging for drug targeting to the brain since most pharmaceutical candidates end up in lysosomes instead of being transcytosed across the brain endothelial cell barrier (Toth et al. 2019). To show a therapeutic potential, the polymer has to be endocytosed on the lumen side, trafficked through the cell and released on the brain side.

To analyze if the polymers were transported from the luminal surface of the endothelial cells (bEnd.3) to the abluminal surface, an *in vitro* BBB transport assay was performed. First, the integrity of the endothelial barrier was determined using impedance measurements to calculate the transendothelial electrical resistance (TEER) and cell capacity, shown in figure 19. TEER and capacity values were determined automatically during the whole experiments every hour by the CellZscope device. Immediately after the application of the polymers or the control, the TEER values increased but then decreased and did not fall below the initial value. By applying the control and samples, the TEER is increasing caused by an artifact of the measurement. The electrodes of the CellZscope measure the ions compared to the initial conditions. By applying the samples and control with new media, the TEER is increasing. If the values are decreasing back to the initial values, the integrity of the barrier can be assumed to be intact after polymer application. Caused by the high TEER values and capacity of the controls, the axes would be on a larger scale, and the lower TEER and capacity values from the samples would not be visible anymore. Therefore, the TEER (y-axis) scale was set to 100 Ωcm^2, and the scale for the capacity (y-axis) was set to 10 $\mu F/cm^2$.
Furthermore, the high TEER for the control (A1) of figure 19 b) seems to be a technical artifact (e.g. an air bubble) because the TEER is increasing drastically after the application and is decreasing after four hours to the initial value. Also, the capacity of A1 is falling below the initial value and recovers over time. Overall after recovering the control A1, the membrane seems to be intact. Only the TEER measurement of the control C2 is consistently too high after

application, and therefore cannot be assumed to be reliable. If the barrier would not remain intact, the TEER would decrease, caused by the opening of the TJ of the endothelial cells. The capacity does not change when the barrier is not intact because the polymer can diffuse paracellularly between the cells in to the abluminal compartment.

In all three measurements of figure 19 (b, c, and d), it can be seen that the polymer does not trigger any cell stress and that the integrity of the barrier remains intact.

In figure 20 is shown the transportation rates of the polymers in percent from a luminal compartment into an abluminal compartment. The quantification of the transport revealed for PD-Cy5 99 ± 23.91 %, PDD-Cy5 109 ± 16.29 %, and for PLD-Cy5 122 ± 13.42 % (figure 20), compared to an insert without cells set to 100 % of transport. These transport rates are unexpectedly high and are different from an earlier transport assay with a different batch of polymers, done by Dr. Jana Hedrich.

The observed high transport of the polymer (while having an intact barrier) could be due to unbound Cy5 fluorophore or a smaller polymer size due to degradation of the polymers. One option to test if the samples are containing unbound Cy5 fluorophore is using High-performance liquid chromatography (HPLC) or Mass spectrometry (MS). According to this, further experiments on the transportation rate have to be investigated.

In principle, actual transportation above 100% (while having an intact barrier) could be possible through active transport mechanisms of the polymers by the endothelial cell. The transport rate of PLD-Cy5 122 ± 13.42 % is higher compared to the control, which could be explained due to active transport. Overall, the possibility of polymers transportation through an intact barrier of mouse endothelial cell line bEnd.3 could not be quantified without a doubt yet and has to be further investigated.

In physiological conditions, after a successful transport through the endothelial cells, the polymer reaches the brain parenchyma and comes in contact with neuronal cells. To examine the polymers ability to be delivered to neurons and astrocytes, I have studied the uptake into target cells by using immunocytochemistry on murine primary cultures after polymers treatment for 24 hours.

In figures 13, 14, and 15, the positive polymer signal (magenta) is shown in every cell. Despite an increase in the concentration of the application of the polymer (from 50 µg/ml to 200 µg/ml), no increased uptake of the polymer into the cells could be determined. This is fundamentally different from the uptake of the polymer into the endothelial cell line bEnd.3. The reasons for no concentration-related uptake of the polymer by increasing the polymer concentration into

neuronal cell culture would be a topic for future investigations. So far, it can only be hypothesized that the poly polymers lowest applied concentration of 50 µg/ml was already saturating the cell uptake. With further increasing polymer concentrations, either the cells do not take up more polymers, or polymer degradation or metabolism starts. Differences in uptake characteristics for the respective polymers (PD-Cy, PDD-Cy5, and PLD-Cy5) could not be determined.

To investigate the uptake of the target cells in the NVU, I have antibody stained different cell types. Therefore, astrocytes were stained with marker glial fibrillary acidic protein (GFAP, green), while neurons were stained with the soma marker (NeuN, red). Both stainings were visualized in figures 16, 17, and 18. The polymer signal (magenta) can be determined in the neurons (red) and the astrocytes (green), shown in figures 16, 17, and 18. The localization of the polymer signal in neurons and astrocytes can be assumed by the uptake related to the polymers size and charge. Overall, it could be detected that the polymers were well uptaken into the target cells which could increase the potential as a therapeutic treatment.

4.2 Comparison of polymer and monomer toxicity

The currently used treatment for PD is levodopa (L-DOPA) administration to the patient. L-DOPA can cross the BBB and will be converted into dopamine inside the brain parenchyma (B. Sampaio-Maia et al.; Cheng et al. 2010; Meiser 2013). Therefore, the lack of dying dopaminergic (DA) neurons in the midbrain is compensated by replacing dopamine. But only 1% of the administered L-DOPA reaches the intact brain, which leads to high administrations of L-DOPA (Vong et al. 2020).

In this study, the toxicity of the polymers compared to monomers of dopamine, L-DOPA and D-DOPA were investigated as a potential improvement compared to the monomers. At first, the toxicity of the polymers on endothelial cells (bEnd.3) was investigated. In figure 21, the highest viability is demonstrated with the lowest concentration of 25 µg/ml and for PLD (orange) 138 ± 4 %, PD (blue) 116 ± 10 %, and PDD (green) 90 ± 3 %. With the concentration of 25 µg/ml, the viability of PD (116%) and PDD (90%) are not higher compared to the control due to the overlapping error bars (figure 21). Vitality values higher than 100 % were observed for PLD 25 and 50 µg/ml and will be discussed. The viability was measured by determining the number of viable cells by quantifying the present ATP amount, which indicates the presence of active metabolic cells, with CellTiter-Glo (Riss et al. 2001). One reason for vitality values

higher than the 100 percent control group could be different cell numbers in the tested samples. To exclude this, the measurement should be repeated several times (at least three times), and the seeding of the 96-well plate should be discontinues as the application of the polymers. Each sample was measured in triplicates, so one sample should be applied on cells seeded at the beginning of the plate, the second should be applied on cells seeded in the middle, and the third on cells seeded at the end of the plate. In addition, sedation of the cells in the stock solution should be avoided and continuously homogeneous.

Another explanation could be a change of metabolism due to the polymers treatment, which could increase the ATP amount. Moreover, it is known that the brain endothelium expresses a variation of adenosine triphosphate (ATP)-driven efflux pumps (Mikitsh and Chacko 2014). These pumps actively transport substances from the endothelial cells back into the bloodstream or into the brain parenchyma (Dickens et al. 2016). Therefore, it could be assumed, by effluxing substances from the ATP-driven efflux transporters in endothelial cells, a higher metabolism is leading to higher ATP levels, which could be above the 100 % control. According to the data in figure 21, the high viability rates of 25 µg/ml PLD (138 ± 4 %) and 50 µg/ml PLD (123 ± 8 %) might be explained by high efflux activity.

With a 600 µg/ml concentration, the viability is the lowest for PLD with 39 ± 4 % and PDD 43 ± 3 %. At the concentration of 400 µg/ml, the viability of PD is the lowest with 71 ± 3 %. However, a clear statement can be made that a higher polymer concentration leads to an increase in toxicity in bEnd.3 cells. Otherwise, a lower concentration of the polymer is less harmful and leads to higher viability. Therefore, the concentration-related toxicity of the polymer on endothelial cells could be observed.

Caused by the known toxicity of the monomers (L-DOPA) to the brain, (Vong et al. 2020), the toxicity of the monomers on endothelial cells (bEnd.3) was investigated to analyze any differences in terms of toxicity between the monomers and polymers. In figure 22 is shown, the highest viability with the lowest concentration of 25 µg/ml LD (orange, 99 ± 3 %), D (88 ± 4 %), and DD (46 ± 1 %). With a 600 µg/ml concentration, the viability is the lowest for every sample. The lowest viability of LD is 10 ± 0 %, and for DD and D 0 ± 0 %. Overall, the concentration-related toxicity of the monomers on endothelial cells (bEnd.3) could be revealed.

Furthermore, the toxicity of polymers (figure 21) compared to the monomers (figure 22) was investigated. To compare the viability or the toxicity between polymers and monomers, the concentrations of monomers in the polymers must be considered. The polymer is built by 40 % polymerized monomer and 60 % PEG 3000. Therefore, a concentration of 100 µg/ml

polymer equals 40 µg/ml of the monomer. Thus, the toxicity of the concentration of 50 µg/ml monomer (figure 22) was assumed by the concentration of 40 µg/ml monomer, to compare the assumed toxicity (40 µg/ml monomer) with the measured toxicity of the concentration of 100 µg/ml of its polymer (figure 21). Also, the toxicity of 240 µg/ml monomer was assumed to equal the measured toxicity of 600 µg/ml of its polymer. With the concentration of 40 µg/ml dopamine (D), the toxicity of 24 % was assumed. The measured toxicity of its polymer (polydopamine, PD) with 100 µg/ml concentration was 6 %. The assumed toxicity of 240 µg/ml dopamine revealed 104 %, and the measured toxicity of 600 µg/ml PD showed 19 %. This is indicating higher toxicity of dopamine compared to polydopamine on endothelial cells. With a concentration of 40 µg/ml and 240 µg/ml D-DOPA, the toxicity of 45 % and 92 % was assumed. The measured toxicities for poly(D-DOPA) of 100 µg/ml and 600 µg/ml revealed 17 % and 57 %. This is also suggesting higher toxicity of D-DOPA compared to poly(D-DOPA). The assumed toxicities for 40 µg/ml and 240 µg/ml L-DOPA revealed 4% and 36%. For poly(L-DOPA), the measured toxicities of 100 and 600 µg/ml showed 13 % and 61%. Therefore, higher toxicity for PLD on endothelial cells could be observed.
However, the experiment should be repeated at least three times. Therefore, further investigations must be taken. Overall, if the polymers would reveal lower toxicity on endothelial cells than the monomers, they would show higher biocompatibility.

Further, the viability of the polymers compared to the monomers was tested on neuronal cell culture (figure 23). The concentration of 100 µg/ml polymer equals the concentration of 40 µg/ml monomer, as prior described. In figure 23 it was applied polymer batch three (from 08.08.20) on neuronal cells (prepared 09.09.20) on 18.09.20. All polymers are showing similar viabilities (PD 52 ± 4 %, PDD 48 ± 1 %, and PLD 48 ± 6 %). The viability of DD is the lowest (22 ± 4 %), compared to D (35 ± 16 %) and LD (31 ± 5 %). Due to the overlapping error bars of dopamine and polydopamine, no clear difference in viability could be observed but is showing a high variation of the measurements. The error bars of DD, PLD, LD, and PLD are different in their viabilities. This indicates lower viability for DD and LD than PDD and PLD or otherwise higher toxicity for DD and LD than PDD and PLD.
After repeating the experiments, a variation of the polymers viability could be observed. In figure 24 is shown the viability of a three-month-old polymers batch on neuronal cells. It was applied on the 2021-01-10 batch four (from 2020-11-12) on neuronal cells (prepared 2021-01-12). With a concentration of 100 µg/ml on the cells, the viability of all samples is below 45 %. For PD the viability is 41 ± 3 %, PDD 23 ± 4 %, and PLD 33 ± 9 %. Therefore, the lower

viability of the neurons treated with the older batch (figure 24) compared to the neurons treated with a new polymer batch (figure 23) could be observed. Consequently, the endotoxin pollution of the polymers was analyzed, which could cause the higher toxicity of the older polymer batch. Endotoxins are a part of the outer cell membrane of gram-negative bacteria or cyanobacteria and a type of lipopolysaccharide (LPS). The toxicity of the LPS depends on the composition of the lipid, which is depending on the environmental conditions. Soluble endotoxin will be released when the bacteria are destroyed, but also physiologically as membrane vesicles.
In table 3, the endotoxin pollution of the polymers batch four from 2020-11-12 is shown. The lower endotoxin pollution of the unlabeled samples (PD, PDD, and PLD) could be observed. Otherwise, the higher endotoxin burden of the Cy5 labeled samples is visible (PD-Cy5, PDD-Cy5, and PLD-Cy5). Overall, in at least batch four, endotoxin pollution could be investigated (table 3).
Endotoxins are associated with neurodegenerative diseases, partly because of their toxicity. The endotoxin hypothesis is hypostasizing a non-genetic stimulus, endotoxin causes or contributes to neurodegeneration (Brown et al. 2019). In healthy patients, the endotoxin in the plasma is about 1 and 50 pg/ml, and the highest endotoxin levels are shown in patients with sepsis with a concentration of 500 pg/ml (Opal et al. 1999; Brown et al. 2019). An increase of 10 pg endotoxin/ml to human blood is enough to activate monocytes and endothelial cells (Erridge et al. 2007). Consequently, a relatively mild blood endotoxin dose can cause acute microglial activation within the brain (Brown et al. 2019). Due to the risks of endotoxins, the Food and Drug Administration (FDA) set the limits for endotoxin in medical devices to be less than 0.5 EU/ml unless the device is coming into contact with the cerebrospinal fluid where the limit is 0.06 EU/ml.

The neurotoxicity increase from a fresh polymer batch (figure 23) to the three-month-old batch (figure 24), and the measured endotoxin concentrations do not correlate (table 3). This is because the neurotoxicities of figures 23 and 24 were measured with different polymer batches. The neurotoxicity of figure 23 was measured with polymer batch three, and the neurotoxicity of figure 24 was measured with batch four. Only the endotoxin pollution of batch four was analyzed. Therefore, we can not make an assessment of the endotoxin load of the neurons treated with batch three, shown in figure 23. The highest endotoxin pollution in batch four was demonstrated in the Cy5 labeled samples, but these were not used in the neurotoxicity assays.

In the unlabeled samples (which were applied to the primary neurons), the highest toxicity was found in polydopamine (3,5844 EU/ml). The pollution for PLD was 0,9064 and for PDD 0,7880 EU/ml. Therefore the endotoxin pollution in the PD sample is at least three times higher compared to PLD and PDD.
Additionally, we have to consider that the quality of the neurons in the different assays is having a real impact on the assay outcome. Further, the measured neurotoxicity of batch four in figure 24 was done on 2021-01-12, and the endotoxin pollution was analyzed four weeks later (2021-02-09). Therefore, contamination with bacteria could lead to higher endotoxin pollution of the batch during these four weeks.

In conclusion, this highlights that it is mandatory to investigate any further experiments only with endotoxin-free polymer solutions. The very first step would be preventing endotoxin. Therefore, it would be helpful only to use high-purity water to prepare medium and for washing steps (e.g., glassware). Also, water purification systems, water storage containers, and associated tubing should be maintained to prevent significant levels of endotoxin-producing bacteria. Overall, it would be helpful to synthesize the polymers under sterile conditions to avoid bacterial contamination of the polymers batch, although sterile production of the polymers can prove challenging. Therefore, an adequate way of purifying endotoxin-contaminated substances should also be available, even if it is known that endotoxins are considered temperature and pH stable, which hardens their removal as one of the most difficult during protein purification (Magalhães et al. 2007). Overall the currently used methods are either non-selective, toxic, or expensive (Ongkudon et al. 2012 2012). Common ways for decontaminating endotoxins are endotoxin removal kits, ultrafiltration, and ion-exchange chromatography (Sweander et al. 1997; Shibatani et al. 1983; Magalhães et al. 2007), or affinity ligands based on the immobilized amino acids. For example, L-histidine (non-selective), endotoxin binding proteins (very expensive), or polymyxin B (toxic) (Ongkudon et al. 2012 2012)

4.3 In vitro Parkinson disease model with concentration related dopamine rescue

As prior in chapter 1.8 “The dilemma of Parkinson disease” described, the depletion of dopamine in the nigrostriatal pathway is the main pathological hallmark (Laloux et al. 2017). To investigate an *in vitro* PD model, I have introduced neurotoxicity into neuronal cell culture by using 10 µM 1- methyl-4-phenylpyridinium (MPP^+) (Laloux et al. 2017).

In figure 25 is demonstrated the dopamine concentration-related rescue of *in vitro* Parkinson disease neurons. MPP^+ was applied on neuronal cells and incubated for 24 h. One day after, I have applied dopamine (D) in different concentrations (0.05, 0.1, and 0.2 µM D) and also a control (only neurons medium). The control without MPP^+ was used to visualize a “positive” control, that the neurons were grown fine without any neurotoxic substances. The viability of the control without MPP^+ was the highest and set to 100 % (100 ± 18 % for 3 samples). The samples treated with MPP^+ and dopamine showed a concentration-related rescue of the neurons by highering dopamine concentration. Therefore, the highest toxicity was measured by the lowest application of 0.05 µM D 19 ± 5 %. The viability increased with the application of 0.1 µM D to 26 ± 2 %, and the highest viability was measured with the highest dopamine application of 0.2 µM with 49 ± 9 %. Moreover, a control with MPP^+ and only neurons medium, without dopamine, was used to show the “negative” control. The viability of the MPP^+ medium neurons (without dopamine) was one of the lowest 21 ± 3 %. The MPP^+ medium sample shows that dopamine is rescuing the neurons by applying and increasing dopamine concentrations, higher viabilities compared to the viability of the MPP^+ medium sample being shown.

Further, it could be observed that the herein used concentrations of dopamine are too low. The viabilities of the highest dopamine application (0.2 µM) revealed 49 ± 9 %. Therefore, it should be further investigated if higher dopamine concentrations are rescuing more neurons and revealing higher viabilities. Overall in figure 25 could be visualized the rescue of the *in vitro* PD neurons by the application of a higher dopamine concentration (up to 0.2 µM).

Overall by addressing the scientific questions at the beginning of my thesis, polydopamine, poly(D-DOPA), and poly(L-DOPA) were uptaken into endothelial (bEnd.3) and neuronal cells. The polymer signal in b.End cells were concentration-related and shown in EE, cytosol, unknown vesicles, and LE. Further, the uptake into the target cells could be observed by colocalization of the polymer signal in neurons and astrocytes (1). The transport *in vitro* from the luminal (blood side) to the abluminal (brain side) could not be proven yet. Further, it could be observed that the polymers are not triggering any cell stress and that the integrity of the brassier remains intact after polymer application (1). Moreover, the transcytosis pathway was assumed by endosomal transport of the polymers in early and late endosomes. Polymer signal in the cytosol and unknown vesicles was also observed. (2). Moreover, the polymers influence the viability of the NVU cells, but less than the monomers and the integrity of the BBB is still intact after polymer application *in vitro* (3). Additionally, the influence of the endotoxins in the polymer batch on the viability of the neurons could be observed, highlighting the need for endotoxin-free polymer batches.

5 Outlook

In further experiments, the PD *in vitro* model should be optimized. Therefore, a higher concentration of dopamine should be tested, because the herein used highest concentration of 0.2 µM showed only viability of 49 ± 9 % compared to 21 ± 3 % of MPP^+ treated neurons, and a rescue to nearly 100 % is aimed for. Also, this experiment should be further used to investigate the rescue of the neurons by applying the polymers (in optimal concentrations). Moreover, the rescue of the *in vitro* PD neurons with polymers and monomers should be compared. An advantage of polymers compared to the monomers would be lower neurotoxicity, which was observed for PDD and PLD in figure 23. Additionally, it should be investigated if the polymers are influencing the viability of the astrocytes. Therefore, a neurotoxicity assay which was not treated with araC (cytosine arabinofuranoside) should be investigated. In the prior tested neurotoxicity assay the cultures were treated with araC, to inhibit the proliferation of glia cells to yield a "neuron-only" culture.

Another advantage of the polymer in contrast to the monomer could be the lower toxicity on endothelial cells, which was indicated by the experiments in figure 21 and 22. Moreover, a different vitality marker instead of ATP metabolism should be used for endothelial cells to exclude falsified viability rates due to the ATP-driven efflux pumps. Furthermore, a toxicity marker instead of a viability marker could quantify the polymers effects independent of ATP levels.

In addition, the polymer transport rates through a confluent layer of endothelial cells should be examined again after excluding free Cy5 fluorophore or polymer degradation in the polymer batch used. Since the transport rates of the herein measured batches are high and around 100 %, and additionally not correlating to prior experiments.

Moreover, the trafficking of the polymers in brain endothelial cells should be investigated in more detail. Therefore, the uptake of the polymers should be antibody stained with different markers for the transcytose pathway. Since the herein shown data let assume the endocytosis of the polymer in early endosomes, localization of polymer signal in the cytosol and late endosomes, as well as unknown vesicles. Additionally, a known substance with a known transcytosis pathway could be used as a marker to analyze if the polymer signal colocalizes with the known pathway, this would indicate that the pathways are the same, if not this pathway could be excluded. Overall, all of the experiments should be repeated several times, to develop stable data.

After a successful *in vitro* transport, the transport should be analyzed and ideally quantified in an *in vivo* model since *in vitro* models will never meet physiological conditions in the brain. If the polymer is successfully transported across the BBB *in vivo*, it should be investigated if it is metabolized on the brain side and reveals functional unites, by using for example MALDI mass spectrometry. Are most of these experiments describe *in vitro* assays, with promising results the polymers still have to be studied *in vivo* in a PD model. In conclusion, there could be a promising potential of polymers as a therapeutic treatment for Parkinson disease, which has to be further evaluated.

6 References

Abbott, N. Joan (1986): The Blood-Brain Interface in Invertebrates.

Abbott, N. Joan (2003): Dynamics of CNS barriers: evolution, differentiation, and modulation. In *Cellular and molecular neurobiology* 25 (1), pp. 5–23. DOI: 10.1007/s10571-004-1374-y.

Abbott, N. Joan; Patabendige, Adjanie A. K.; Dolman, Diana E. M.; Yusof, Siti R.; Begley, David J. (2010): Structure and function of the blood-brain barrier. In *Neurobiology of disease* 37 (1), pp. 13–25. DOI: 10.1016/j.nbd.2009.07.030.

Armulik, Annika; Abramsson, Alexandra; Betsholtz, Christer (2005): Endothelial/pericyte interactions. In *Circulation research* 97 (6), pp. 512–523. DOI: 10.1161/01.RES.0000182903.16652.d7.

Armulik, Annika; Genové, Guillem; Betsholtz, Christer (2011): Pericytes: developmental, physiological, and pathological perspectives, problems, and promises. In *Developmental cell* 21 (2), pp. 193–215. DOI: 10.1016/j.devcel.2011.07.001.

Armulik, Annika; Genové, Guillem; Mäe, Maarja; Nisancioglu, Maya H.; Wallgard, Elisabet; Niaudet, Colin et al. (2010): Pericytes regulate the blood-brain barrier. In *Nature* 468 (7323), pp. 557–561. DOI: 10.1038/nature09522.

Artursson et al. (1990): Epithelial transport of drugs in cell culture. I: A model for studying the passive diffusion of drugs over intestinal absorptive (Caco-2) cells. In *Journal of pharmaceutical sciences* 79 (6), pp. 476–482. DOI: 10.1002/jps.2600790604.

B. Sampaio-Maia; M. P. Serrão; and P. Soares-da-Silva: Regulatory pathways and uptake ofL-DOPA by capillary cerebral endothelial cells, astrocytes, and neuronal cells 2000.

Balestrino, R.; Schapira, A. H. V. (2020): Parkinson disease. In *European journal of neurology* 27 (1), pp. 27–42. DOI: 10.1111/ene.14108.

Battaglini, Matteo; Marino, Attilio; Carmignani, Alessio; Tapeinos, Christos; Cauda, Valentina; Ancona, Andrea et al. (2020): Polydopamine Nanoparticles as an Organic and Biodegradable Multitasking Tool for Neuroprotection and Remote Neuronal Stimulation. In *ACS applied materials & interfaces* 12 (32), pp. 35782–35798. DOI: 10.1021/acsami.0c05497.

Bellavance, Marc-André; Blanchette, Marie; Fortin, David (2008): Recent advances in blood-brain barrier disruption as a CNS delivery strategy. In *The AAPS journal* 10 (1), pp. 166–177. DOI: 10.1208/s12248-008-9018-7.

Bridi, Jessika C.; Hirth, Frank (2018): Mechanisms of α-Synuclein Induced Synaptopathy in Parkinson's Disease. In *Frontiers in neuroscience* 12, p. 80. DOI: 10.3389/fnins.2018.00080.

Brown et al. (2019): The endotoxin hypothesis of neurodegeneration. In *Journal of neuroinflammation* 16 (1), p. 180. DOI: 10.1186/s12974-019-1564-7.

Brune, Karl D.; Leneghan, Darren B.; Brian, Iona J.; Ishizuka, Andrew S.; Bachmann, Martin F.; Draper, Simon J. et al. (2016): Plug-and-Display: decoration of Virus-Like Particles via isopeptide bonds for modular immunization. In *Scientific reports* 6, p. 19234. DOI: 10.1038/srep19234.

Cheng, Hsiao-Chun; Ulane, Christina M.; Burke, Robert E. (2010): Clinical progression in Parkinson disease and the neurobiology of axons. In *Annals of neurology* 67 (6), pp. 715–725. DOI: 10.1002/ana.21995.

Dallas, Shannon; Miller, David S.; Bendayan, Reina (2006): Multidrug resistance-associated proteins: expression and function in the central nervous system. In *Pharmacological reviews* 58 (2), pp. 140–161. DOI: 10.1124/pr.58.2.3.

Daneman, Richard; Zhou, Lu; Kebede, Amanuel A.; Barres, Ben A. (2010): Pericytes are required for blood-brain barrier integrity during embryogenesis. In *Nature* 468 (7323), pp. 562–566. DOI: 10.1038/nature09513.

Dickens et al. (Ed.) (2016): Drug transporters. Royal Society of Chemistry (Great Britain). Cambridge: Royal Society Of Chemistry (RSC drug discovery series, no. 54-55).

Erridge, Clett; Attina, Teresa; Spickett, Corinne M.; Webb, David J. (2007): A high-fat meal induces low-grade endotoxemia: evidence of a novel mechanism of postprandial inflammation. In *The American journal of clinical nutrition* 86 (5), pp. 1286–1292. DOI: 10.1093/ajcn/86.5.1286.

Gaillard et al. 2000: PII: S0928-0987(00)00152-4.

Greffard, Sandrine; Verny, Marc; Bonnet, Anne-Marie; Beinis, Jean-Yves; Gallinari, Claude; Meaume, Sylvie et al. (2006): Motor score of the Unified Parkinson Disease Rating Scale as a good predictor of Lewy body-associated neuronal loss in the substantia nigra. In *Archives of neurology* 63 (4), pp. 584–588. DOI: 10.1001/archneur.63.4.584.

Harvey, Sean; Ng, David Yuen Wah; Szelwicka, Jolanta; Hueske, Lisa; Veith, Lothar; Raabe, Marco et al. (2018): Facile synthesis of ultrasmall polydopamine-polyethylene glycol nanoparticles for cellular delivery. In *Biointerphases* 13 (6), 06D407. DOI: 10.1116/1.5042640.

Hilker, Ruediger; Schweitzer, Katherine; Coburger, Silke; Ghaemi, Mehran; Weisenbach, Simon; Jacobs, Andreas H. et al. (2005): Nonlinear progression of Parkinson disease as determined by serial positron emission tomographic imaging of striatal fluorodopa F 18 activity. In *Archives of neurology* 62 (3), pp. 378–382. DOI: 10.1001/archneur.62.3.378.

Kaech, Stefanie; Banker, Gary (2006): Culturing hippocampal neurons. In *Nature protocols* 1 (5), pp. 2406–2415. DOI: 10.1038/nprot.2006.356.

Kalia, Lorraine V.; Kalia, Suneil K.; Lang, Anthony E. (2015): Disease-modifying strategies for Parkinson's disease. In *Movement disorders : official journal of the Movement Disorder Society* 30 (11), pp. 1442–1450. DOI: 10.1002/mds.26354.

Kamphorst (2002): ulmonary mucinous cystic tumour of borderline Pulmalignancy: a rare variant of adenocarcinoma 2002.

Keller, Annika (2013): Breaking and building the wall: the biology of the blood-brain barrier in health and disease. In *Swiss medical weekly* 143, w13892. DOI: 10.4414/smw.2013.13892.

Kijanska, Monika; Kelm, Jens (2004): Assay Guidance Manual. In vitro 3D Spheroids and Microtissues: ATP-based Cell Viability and Toxicity Assays. Edited by Sarine Markossian, G. Sitta Sittampalam, Abigail Grossman, Kyle Brimacombe, Michelle Arkin, Douglas Auld et al. Bethesda (MD).

Koh, J. Y.; Wie, M. B.; Gwag, B. J.; Sensi, S. L.; Canzoniero, L. M.; Demaro, J. et al. (1995): Staurosporine-induced neuronal apoptosis. In *Experimental neurology* 135 (2), pp. 153–159. DOI: 10.1006/exnr.1995.1074.

Kuhnert (2010): Essential Regulation of CNS Angiogenesis by the Orphan G Protein–Coupled Receptor GPR124. In *Science (New York, N.Y.)* 330 (6006), pp. 982–985. DOI: 10.1126/science.1194134.

Laloux, C.; Gouel, F.; Lachaud, C.; Timmerman, K.; Do Van, B.; Jonneaux, A. et al. (2017): Continuous cerebroventricular administration of dopamine: A new treatment for severe dyskinesia in Parkinson's disease? In *Neurobiology of disease* 103, pp. 24–31. DOI: 10.1016/j.nbd.2017.03.013.

Magalhães, Pérola O.; Lopes, André M.; Mazzola, Priscila G.; Rangel-Yagui, Carlota; Penna, Thereza C. V.; Pessoa, Adalberto (2007): Methods of endotoxin removal from biological preparations: a review. In *Journal of pharmacy & pharmaceutical sciences : a publication of the Canadian Society for Pharmaceutical Sciences, Societe canadienne des sciences pharmaceutiques* 10 (3), pp. 388–404.

Meiser (2013): Complexity of dopamine metabolism.

Mikitsh, John L.; Chacko, Ann-Marie (2014): Pathways for small molecule delivery to the central nervous system across the blood-brain barrier. In *Perspectives in medicinal chemistry* 6, pp. 11–24. DOI: 10.4137/PMC.S13384.

Miller, David S. (2010): Regulation of P-glycoprotein and other ABC drug transporters at the blood-brain barrier. In *Trends in pharmacological sciences* 31 (6), pp. 246–254. DOI: 10.1016/j.tips.2010.03.003.

Montesano, R.; Pepper, M. S.; Möhle-Steinlein, U.; Risau, W.; Wagner, E. F.; Orci, L. (1990): Increased proteolytic activity is responsible for the aberrant morphogenetic behavior of endothelial cells expressing the middle T oncogene. In *Cell* 62 (3), pp. 435–445. DOI: 10.1016/0092-8674(90)90009-4.

Moscariello (2018): In vitro and in vivo investigation of dendronized streptavidin and fluorescent nanodiamonds, two flexible nanosystems efficiently crossing the blood-brain barrier to improve nanotheranostics in neurological disease treatment.

Neuwelt, Edward A.; Bauer, Björn; Fahlke, Christoph; Fricker, Gert; Iadecola, Constantino; Janigro, Damir et al. (2011): Engaging neuroscience to advance translational research in brain barrier biology. In *Nature reviews. Neuroscience* 12 (3), pp. 169–182. DOI: 10.1038/nrn2995.

Nimmerjahn (2005): Resting Microglial Cells Are Highly Dynamic Surveillants of Brain Parenchyma in Vivo. In *Science (New York, N.Y.)* 308 (5726), pp. 1310–1314. DOI: 10.1126/science.1107891.

Ongkudon et al. 2012 (2012): Chromatographic Removal of Endotoxins: A Bioprocess Engineer's Perspective. In *ISRN Chromatography* 2012 (3), pp. 1–9. DOI: 10.5402/2012/649746.

Opal, S. M.; Scannon, P. J.; Vincent, J. L.; White, M.; Carroll, S. F.; Palardy, J. E. et al. (1999): Relationship between plasma levels of lipopolysaccharide (LPS) and LPS-binding

protein in patients with severe sepsis and septic shock. In *The Journal of infectious diseases* 180 (5), pp. 1584–1589. DOI: 10.1086/315093.

Pardridge, William M. (2001): Brain drug targeting. The future of brain drug development. Cambridge: Cambridge University Press.

Riss et al. 2001: CellTiter-Glo™ Luminescent Cell Viability Assay: A Sensitive and Rapid Method for Determining Cell Viability.

Sardoiwala, Mohammed Nadim; Srivastava, Anup K.; Kaundal, Babita; Karmakar, Surajit; Choudhury, Subhasree Roy (2020): Recuperative effect of metformin loaded polydopamine nanoformulation promoting EZH2 mediated proteasomal degradation of phospho-α-synuclein in Parkinson's disease model. In *Nanomedicine : nanotechnology, biology, and medicine* 24, p. 102088. DOI: 10.1016/j.nano.2019.102088.

Schünke, Michael; Schulte, Erik; Schumacher, Udo; Voll, Markus; Wesker, Karl (2015): Prometheus Lernatlas - Kopf, Hals und Neuroanatomie. 4., überarbeitete und erweiterte Auflage. Stuttgart: Thieme (Thieme eRef). Available online at https://eref.thieme.de/ebooks/1224001.

Shibatani, Takeji; Kakimoto, Toshio; Chibata, Ichiro (1983): Purification of High Molecular Weight Urokinase from Human Urine and Comparative Study of Two Active Forms of Urokinase. In *Thromb Haemost* 49 (02), pp. 91–95. DOI: 10.1055/s-0038-1657329.

Spillantini (1997): Î-Synuclein in Lewy bodies.

Sweander et al. 1997: Applied and Environmental Microbiology-1977-Sweadner-382.full.

Toth, Andrea E.; Nielsen, Simone S. E.; Tomaka, Weronika; Abbott, N. Joan; Nielsen, Morten S. (2019): The endo-lysosomal system of bEnd.3 and hCMEC/D3 brain endothelial cells. In *Fluids and barriers of the CNS* 16 (1), p. 14. DOI: 10.1186/s12987-019-0134-9.

Trépanier, L. L.; Kumar, R.; Lozano, A. M.; Lang, A. E.; Saint-Cyr, J. A. (2000): Neuropsychological outcome of GPi pallidotomy and GPi or STN deep brain stimulation in Parkinson's disease. In *Brain and cognition* 42 (3), pp. 324–347. DOI: 10.1006/brcg.1999.1108.

Vong, Long Binh; Sato, Yuna; Chonpathompikunlert, Pennapa; Tanasawet, Supita; Hutamekalin, Pilaiwanwadee; Nagasaki, Yukio (2020): Self-assembled polydopamine nanoparticles improve treatment in Parkinson's disease model mice and suppress dopamine-induced dyskinesia. In *Acta biomaterialia* 109, pp. 220–228. DOI: 10.1016/j.actbio.2020.03.021.

WHO (2006): Neurological Disorders public health challenges. Global burden of neurological disorders estimates and projections. Geneva: World Health Organization.

Wilhelm, Imola; Krizbai, István A. (2014): In vitro models of the blood-brain barrier for the study of drug delivery to the brain. In *Molecular pharmaceutics* 11 (7), pp. 1949–1963. DOI: 10.1021/mp500046f.

Woodfin, Abigail; Voisin, Mathieu-Benoit; Imhof, Beat A.; Dejana, Elisabetta; Engelhardt, Britta; Nourshargh, Sussan (2009): Endothelial cell activation leads to neutrophil transmigration as supported by the sequential roles of ICAM-2, JAM-A, and PECAM-1. In *Blood* 113 (24), pp. 6246–6257. DOI: 10.1182/blood-2008-11-188375.

Wynn, Thomas A.; Chawla, Ajay; Pollard, Jeffrey W. (2013): Macrophage biology in development, homeostasis and disease. In *Nature* 496 (7446), pp. 445–455. DOI: 10.1038/nature12034.

Acknowledgement

First, I would like to thank my group leader Prof. Dr. Tanja Weil, for giving me the opportunity to work on this very comprehensive project. Further I would like to thank my supervisor Dr. Jana Hedrich who has always supported me with her practical and theoretical knowledge. It was a great opportunity to get a deep insight into the working methods and group dynamics of a renowned scientific institute like the Max-Planck institute for polymer research. Furthermore, I want to thank Prof. Dr. Walter Stöcker for agreeing to be the second corrector of my thesis. My special thanks goes to Petya Yordanova, for her help and encouragement. Finally, I want to thank my family (Mama, Papa & André) and my friends (Berin, Ceren, Leticia, Anna, Saskia, Debbie, and all of the others) for their love and support during this special time.